Available online at www.sciencedirect.com

ScienceDirect

Focus Article, *Mendeleev Commun.*, 2023, **33**, 583–596

Mendeleev Communications

Parahydrogen-based NMR signal amplification by reversible exchange (SABRE): recent advances and applications

Oleg G. Salnikov,* Dudari B. Burueva, Ivan V. Skovpin and Igor V. Koptyug

International Tomography Center, Siberian Branch of the Russian Academy of Sciences, 630090 Novosibirsk, Russian Federation. E-mail: salnikov@tomo.nsc.ru

DOI: 10.1016/j.mencom.2023.09.001

Signal amplification by reversible exchange (SABRE) is a rapidly developing nuclear magnetic resonance (NMR) hyperpolarization technique utilizing parahydrogen for dramatic increase of NMR sensitivity to benefit its biomedical and analytic applications. This mini-review covers the most important methodological advances of SABRE with the focus on recent developments. We discuss the mechanistic aspects of SABRE effects, hyperpolarization of protons and heteronuclei including the novel SABRE-Relay approach, the ongoing work to make SABRE biocompatible, the analytical applications, the advances in instrumentation and, finally, more exotic developments such as the low-field detection of SABRE and the SABRE-initiated radiofrequency amplification by stimulated emission of radiation (RASER) effects.

NMR signal amplification by reversible exchange (SABRE)

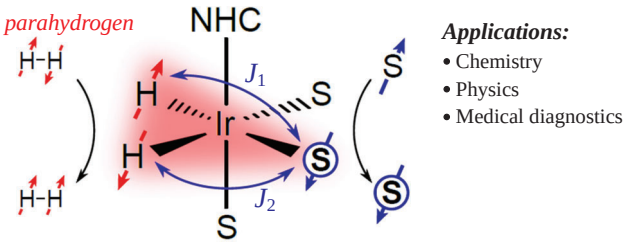

Keywords: NMR spectroscopy, parahydrogen, SABRE, hyperpolarization, magnetic resonance.

Introduction

Nuclear magnetic resonance (NMR) spectroscopy is widely used as a powerful analytical method to probe the structure and reactivity of inorganic and organic compounds, biomolecules, and materials. At the same time, magnetic resonance imaging (MRI) is a highly important diagnostic tool in medicine. The most important disadvantage of NMR and MRI is their intrinsically low sensitivity resulting from the low energy of interactions of the nuclear spins with an external magnetic field, leading to low equilibrium polarization of nuclear spins. In

Oleg G. Salnikov completed his M.Sc. studies in chemistry at Novosibirsk State University in 2014. In 2018 he obtained PhD degree in physical chemistry under the supervision of Dr. Kirill Kovtunov at the International Tomography Center (ITC) SB RAS, employing PHIP technique for the mechanistic studies of heterogeneous catalytic reactions. He continued his research in the group of Prof. Igor Koptyug at ITC SB RAS, where he holds a position of senior research fellow. His research interests are chemical aspects of parahydrogen-based NMR hyperpolarization techniques – PHIP and SABRE – and developments of these techniques toward biomedical applications.

Dudari B. Burueva is currently a research fellow in the group of Prof. Igor Koptyug at the International Tomography Center, Novosibirsk. She received her master's degree in chemistry (2016) as well as her PhD degree in physical chemistry (2021) from Novosibirsk State University. Her research interests include parahydrogen-induced hyperpolarization and its applications for heterogeneous catalysis.

Ivan V. Skovpin graduated from Novosibirsk State University with M.Sc. degree in chemistry in 2010. In 2015 he obtained PhD degree in physical chemistry under the supervision of Dr. Vladimir Zhivonitko at the International Tomography Center (ITC) SB RAS. Currently he is a research fellow in the group of Prof. Igor Koptyug at ITC SB RAS. His research interests include heterogeneous catalysis and parahydrogen-based NMR hyperpolarization techniques – PHIP and SABRE.

Igor V. Koptyug studied physics at the Novosibirsk State University where he received his degree in Chemical Physics in 1985. He then became a junior researcher at the Institute of Chemical Kinetics and Combustion and received his PhD degree in 1991 there. In 1992−1995 he was a postdoctoral researcher in the photochemistry group of Prof. N. J. Turro (Columbia University, New York). Since 1995 he has been working at the International Tomography Center, SB RAS, in various capacities, where he currently holds positions of Head of Research, Chief Research Scientist, and a research group leader. He earned his Dr. Sci. (Habilitation) degree in Catalysis in 2003 and a title of Professor in 2006, and was elected as a Corresponding Member of the Russian Academy of Sciences in 2022. His research interests primarily include signal enhancement in NMR and applications of NMR and MRI in catalysis research.

particular, even in modern 28.2 T NMR spectrometers it does not exceed 0.01%. An elegant solution to this problem is the use of hyperpolarization techniques creating temporary non-equilibrium nuclear spin polarization.[1] Regarding the sensitivity enhancement of liquid-phase NMR, there is a number of hyperpolarization techniques available, the most widely used being dynamic nuclear polarization (DNP),[2,3] parahydrogen-induced polarization (PHIP),[4,5] and signal amplification by reversible exchange (SABRE).[6,7] To introduce the reader into the context of hyperpolarization, we start with a brief description of the most important features of the DNP and PHIP techniques and then move to the detailed coverage of various aspects of SABRE.

DNP is based on the transfer of spin polarization from unpaired electrons to neighboring NMR active nuclei.[1] To hyperpolarize chemicals in solution, usually the dissolution-DNP (d-DNP) approach is used.[8–10] In brief, the sample containing the target chemical and a paramagnetic radical dissolved in a suitable solvents mixture is cooled down to liquid helium temperatures at high magnetic field.[9] The sample composition should provide glass formation with homogeneous distribution of radicals upon freezing. Next, microwave irradiation transfers the electron spin polarization (which is close to unity under these conditions) to the nuclear spins. After sufficient nuclear spin polarization is built up, the sample is rapidly dissolved in hot water and transferred to an NMR spectrometer for detection. d-DNP has found several biomedical applications: compounds hyperpolarized with this technique (*e.g.*, [^{13}C]pyruvate, [U-^{2}H,U-^{13}C]glucose, [^{13}C]acetate) were used in preclinical and clinical studies of metabolism including cancerous tumors.[11–13] However, the high cost of the d-DNP equipment installation and operation and long hyperpolarization cycles significantly limit the widespread use of this approach.

Both PHIP and SABRE techniques use the nuclear singlet spin order of parahydrogen (p-H_2, the singlet nuclear spin isomer of H_2) as a source of nuclear spin hyperpolarization.[14] p-H_2 enrichment of H_2 gas can be performed by cooling it down in the presence of an ortho/para conversion catalyst (usually FeO(OH) or charcoal). 50% Parahydrogen enrichment of H_2 gas can be performed by cooling it down in the presence of an ortho/para conversion catalyst [usually FeO(OH) or charcoal]. The p-H_2 enrichment of 50% can be easily achieved at 77 K using liquid nitrogen,[15] while more advanced setups based on liquid helium cryocooling allow one to obtain ~98–99% p-H_2.[16,17] The produced gas can be stored for a long time at room temperature in an inert (for example, Al) container without back-conversion to normal H_2 (n-H_2) gas (*i.e.*, a 3:1 mixture of ortho- and parahydrogen). Thus, the p-H_2-based hyperpolarization compares favorably with d-DNP in terms of the equipment cost and availability.

The PHIP technique employs p-H_2 in catalytic hydrogenation of unsaturated compounds.[4,18,19] The essential requirement for PHIP is the pairwise addition of two atoms of a single p-H_2 molecule to the same molecule of an unsaturated substrate.[4,20] The PHIP technique has been successfully applied to study the reaction mechanisms of both homogeneous[21] and heterogeneous[19] hydrogenations, and to visualize the processes in model chemical reactors using MRI.[22–24] The development of methods for hyperpolarization transfer from ^{1}H to heteronuclei (for example, ^{13}C) significantly increased its lifetime allowing for the use of PHIP for production of hyperpolarized (HP) molecular contrast agents for biomedical MRI *in vivo*.[25,26] However, the requirement of pairwise hydrogen addition sets limitations on the scope and the applicability of the PHIP technique. Only compounds which have corresponding unsaturated precursors can be directly hyperpolarized by PHIP (although indirect PHIP-SAH[27,28] and PHIP-X[29,30] approaches which in part overcome this issue have been developed, as well as more specific non-hydrogenative parahydrogen-based effects such as oneH-PHIP,[31] pairwise replacement[32–34] and SWAMP[35,36]).

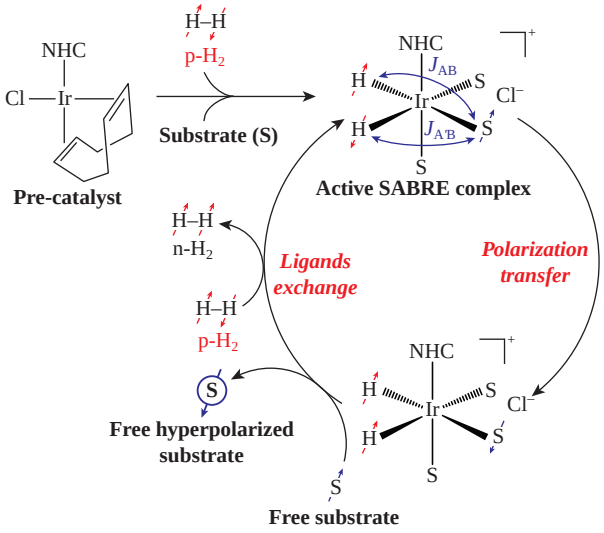

Figure 1 Scheme of polarization transfer and ligands exchange processes in SABRE. NHC is an N-heterocyclic carbene ligand.

The SABRE technique is based on a different way of the use of p-H_2 as a polarization source. In SABRE, both p-H_2 and substrate reversibly bind to a metal (currently – almost exclusively iridium) complex (Figure 1).[6] Within the complex, polarization is transferred from the p-H_2-originated hydride ligands to the substrate nuclear spins. In the 'classic' SABRE experiment, as designed by Adams *et al.*,[6] polarization is spontaneously transferred to the substrate protons at low magnetic fields. The ongoing chemical exchange between the pools of free and metal-bound substrate and hydrogen molecules in solution builds up the hyperpolarization of the free substrate. Thus, unlike PHIP, SABRE does not modify the structure of the hyperpolarized substrate.

Although the SABRE technique is a rapidly developing field of research, there are only few comprehensive reviews[7,37,38] on this topic, the latest of them published in 2019 (there are several more recent reviews but they are more thematically specific,[39] and most of them cover both PHIP and SABRE with the latter one receiving not so much attention).[40–42] Thus, the purpose of this review is to cover various aspects of SABRE with the focus on recent advances in methodology and applications.

Mechanisms of polarization transfer and chemical exchange in SABRE

The SABRE effects result from the complex interplay of both the physical processes of spin dynamics evolution and polarization transfer and the chemical processes of ligands exchange. A detailed description of SABRE physical and chemical models can be found in the dedicated review by Barskiy *et al.*[37] Thus, here we cover only the basics of the mechanistic aspects of SABRE.

The first physical model of spontaneous polarization transfer in the 'classic' ^{1}H SABRE experiments was suggested as early as 2009.[43] Spin dynamics in the four-spin system of the two p-H_2-originated protons and the two protons of the bound substrate was simulated using spin density matrix formalism, considering polarization transfer *via* scalar couplings (*J*-couplings) and chemical shift evolution. As a result, magnetic field profiles of longitudinal magnetization and two-spin order terms as well as zero-quantum (ZQ) coherences were obtained. An alternative and complementary description of polarization transfer in SABRE is based on the concept of level anti-crossings (LACs).[44]

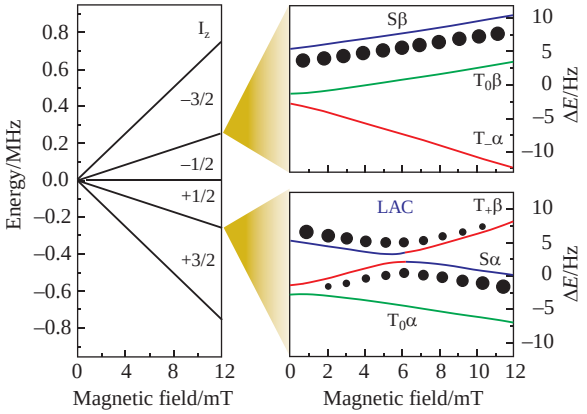

Figure 2 Left panel: spin energy levels of an AA′B spin system with different projections of the total spin I_z. Right panel: the zoom of spin energy levels with $I_z = -1/2$ and $I_z = +1/2$ showing the LAC between the $|T_+\beta>$ and $|S\alpha>$ states. The state populations resulting from the singlet-state preparation of the AA′ spins at different field positions are schematically shown by the solid circles (their size schematically reflects the population of a corresponding state). Calculation parameters: $\delta_A - \delta_B = -30$ ppm, $J_{AA'} = -7$ Hz; $J_{AB} = 2$ Hz, $J_{A'B} = 0$ Hz. Adapted with permission from ref. 45. Copyright (2015) Elsevier Inc.

A LAC occurs at a particular magnetic field where two energy levels tend to cross but the crossing is avoided due to lifting of the degeneracy because of *J*-couplings (Figure 2). Since at the LAC field the eigenstates of the system represent the combinations of the initial states, an efficient exchange of populations of these states takes place. Because the position of the LACs can be easily predicted using NMR parameters of the spin system (chemical shifts and *J*-couplings), this approach allows one to simulate the field dependences of SABRE including the sign of polarization.[44,45]

For the efficient SABRE hyperpolarization, the rates of p-H_2 and substrate chemical exchange should be optimized. Indeed, if exchange is too slow, hyperpolarization is lost due to relaxation processes, while if exchange is too fast, the active complex lifetime is too short rendering polarization transfer inefficient. Thus, later SABRE models aimed to account for both the spin dynamics evolution (including relaxation effects) and the chemical exchange kinetics.[46,47] Barskiy *et al*. derived the 'SABRE formula' describing the dependence of the SABRE signal enhancement on the various experimental parameters (*e.g.*, concentrations, *J*-couplings, exchange, and relaxation rates).[46] It was shown that for low-field SABRE the substrate dissociation rate constant should be close to the spin mixing frequency at the LAC in order to achieve the maximal NMR signal enhancement. Moreover, polarization is proportional to the relaxation time of the bound substrate in the active SABRE complex. Next, Knecht *et al*. presented a SABRE model which combines the exchange kinetics with the spin dynamics evolution and allows one to simulate field profiles of SABRE, multi-spin systems and RF-SABRE experiments.[47] Pravdivtsev and Hövener reported a more advanced model which avoided some of the simplifications used in the previous descriptions of chemical exchange in SABRE.[48] This model provided a master equation that takes into account non-linear chemical and physical dynamics of SABRE multi-spin systems. Next, Lindale *et al*. used infinite-order perturbation theory to assess chemical exchange in SABRE, which provided faster and more accurate simulations of the SABRE dynamics.[49]

While the 'classic' SABRE experiments rely on coherent polarization transfer at low magnetic fields, it was shown that SABRE effects can be also spontaneously created at a high magnetic field of several tesla.[50] The mechanism of spontaneous high-field SABRE was investigated in detail by Knecht *et al*.[51] It was demonstrated that the polarization transfer mechanism consists of three steps: (i) conversion of the singlet spin order of the p-H_2-derived hydrides into anti-phase polarization followed by (ii) its conversion into net magnetization *via* cross-relaxation, finalized by (iii) nuclear Overhauser effect (NOE) polarization transfer from the hydrides to the substrate spins.

In spite of the extensive studies of the SABRE hyperpolarization process, the concomitant ligands exchange

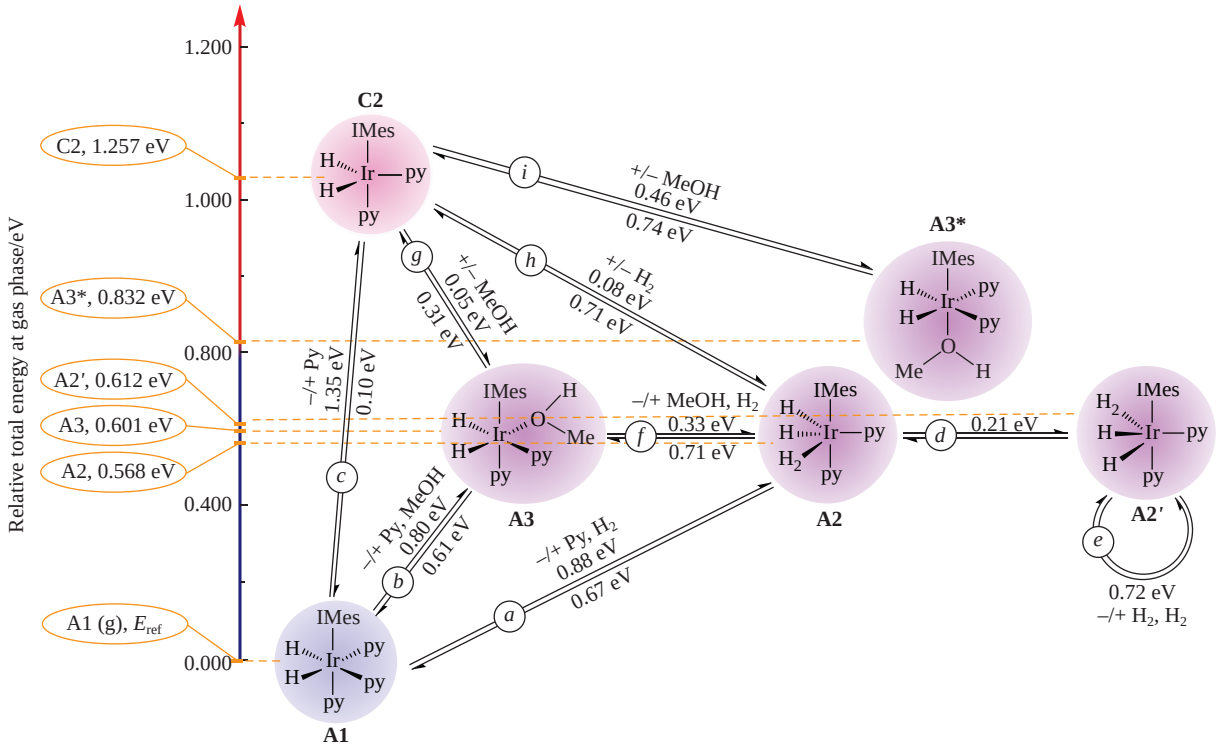

Figure 3 DFT calculations of reaction network for the Ir-IMes catalyst and pyridine SABRE system. Total energies relative to gas phase species for each complex are labeled on the *y*-axis. The calculated energy barriers for the exchange reactions are presented above or below the corresponding reaction arrows. Adapted with permission from ref. 55. Copyright (2021) Wiley-VCH GmbH.

chemistry is not fully understood. Typically, SABRE experiments start with mixing of a substrate S and a SABRE pre-catalyst [Ir(IMes)(COD)Cl] (IMes = 1,3-bis(2,4,6-trimethylphenyl)-imidazol-2-ylidene, COD = 1,5-cyclooctadiene) in CD_3OD solution, resulting in replacement of the chloride ligand with an S molecule to form $[Ir(IMes)(COD)(S)]^+$.[52] Next, upon H_2 introduction oxidative addition of hydrogen to the Ir center occurs, leading to transient hydride species which are then converted to the active SABRE complex $[Ir(IMes)(S)_3(H)_2]^+$ *via* hydrogenation of COD ligand to cyclooctane. As a result, the fully activated SABRE solution contains $[Ir(IMes)(S)_3(H)_2]^+$ as a single species directly detectable by NMR. Indirect chemical exchange saturation transfer (CEST) NMR measurements allowed one to identify $[Ir(IMes)(S)_2(Cl)(H)_2]$ and $[Ir(IMes)(S)_2(CD_3OD)(H)_2]^+$ as minor transient complexes present in the SABRE solution in CD_3OD.[53] Fekete *et al*. showed that despite the low concentrations of these species they can significantly affect the SABRE performance.[54] In particular, temperature variation allows one to manipulate the concentrations of these complexes. Due to the different *J*-coupling networks within the major and the minor SABRE complexes, they differ in the corresponding optimal polarization transfer field. As a result, the appearance of the observed magnetic field profile of SABRE polarization can significantly change with temperature, including the emergence of additional maxima and the shifting of their positions. To identify the plausible ligands exchange pathways in SABRE, Lin *et al*. performed density functional theory (DFT) calculations for the pyridine/Ir-IMes SABRE system.[55] It was found that pyridine exchange predominantly proceeds *via* the replacement of a pyridine (Py) ligand with η^2-H_2 to form $[Ir(IMes)(Py)_2(H_2)(H)_2]^+$ species (dissociative interchange mechanism, Figure 3, reaction *a*). Alternatively, the substrate exchange can proceed *via* an intermediate $[Ir(IMes)(Py)_2(CD_3OD)(H)_2]^+$ species (reactions *b* + *f*), while dissociation of $[Ir(IMes)(Py)_3(H)_2]^+$ to a 16-electron complex $[Ir(IMes)(Py)_2(H)_2]^+$ (as assumed in theoretical SABRE models,[46–48] reaction *c*) was found to be thermodynamically unfavorable. The authors identified H_2/hydride exchange within the Ir coordination sphere (reaction *d*) as a key step of p-H_2 refreshment after polarization transfer from the hydrides to the coordinated substrate.

^{1}H SABRE

Originally, SABRE effects were demonstrated for aromatic heterocyclic compounds with one or more nitrogen atoms (*e.g.*, pyridine, nicotinamide, pyridazine, quinoline, purine, *etc*.) using $[Ir(PCy_3)(S)_3(H)_2]^+$ complex as an active polarization transfer catalyst.[6] Polarization transfer was performed at 20 mT and at the Earth's magnetic field, the maximal ^{1}H polarization ($P_{^1H}$) for pyridine was 3.1%. Further developments of the method have significantly expanded the number of compounds that can be hyperpolarized using SABRE and have optimized experimental conditions, in particular catalyst structure and polarization transfer field. The ligand environment of the iridium center affects the chemical exchange rates (and, hence, the complex lifetime) due to both steric and electronic effects. Variation of the phosphine ligand in the series PCy_3, $PPhCy_2$, PPh_2Cy, PEt_3, $P(Pr^i)_3$, $P(Bu^n)_3$, $P(Bu^t)_3$, and P(1-naphthyl)$_3$ for the $[Ir(PR_3)(Py)_3(H)_2]^+$ complex showed that the highest NMR signal enhancement is observed for the $PPhCy_2$ ligand.[56] Significant increase in attainable polarization (up to 6% net polarization for pyridine) was observed when a phosphine ligand was replaced with a strongly electron-donating and bulky N-heterocyclic carbene (NHC) IMes.[57] Later on, the majority of SABRE studies employed Ir complexes with IMes or other NHC ligands as polarization transfer catalysts. The comparative studies of Ir complexes with various NHC ligands showed that for pyridine, IMes provides the highest SABRE NMR signal enhancement at room temperature as a reflection of optimized substrate exchange rate.[58,59] Several tailored NHC-ligands were also investigated, *e.g.* with a chelating group in one of the aryl moieties.[60–62]

The substituents in the substrate structure also affect the rates of ligand exchange. Stanbury *et al*. studied SABRE hyperpolarization of a number of *para*-substituted pyridines (4-chloropyridine, 4-pyridinecarboxaldehyde methyl hemiacetal, 4-methylpyridine, 4-methoxypyridine).[63] The attainable NMR signal enhancements and exchange rates did not correlate with the substrate p*K*a. However, the temperature dependences of SABRE showed that for all substrates the maximum polarizations are observed under conditions when the bound substrate dissociation rate constant k_d is *ca*. 4–6 s^{-1} (Figure 4). Moreover, the signal enhancement obtained under these optimized conditions clearly correlated with effective T_1 relaxation time of the substrate protons. At the same time, the substrates comparison at the same fixed temperature showed that T_1 correlates with k_d: the higher is k_d, the shorter is the substrate lifetime in the faster relaxing bound state and, thus, the effective T_1 is longer.

The SABRE technique was successfully used to hyperpolarize various nitrogen heterocycles besides pyridine and its derivatives. Duckett *et al*. investigated SABRE hyperpolarization of pyridazine[64] and its derivatives[65] as well as phthalazine.[64] ^{1}H polarization for pyridazine was higher compared to phthalazine (5.2 *vs*. 2.4%) although the ligand exchange rates for both substrates were comparable.[64] The formation of corresponding SABRE-active complexes $[Ir(IMes)(S)_3(H)_2]Cl$ was studied in detail. It was shown that the presence of the –N=N– motif in these heterocycles enables 1,2-metallotropic shift of the coordinated substrate molecules, complicating the chemical exchange network. Next, SABRE of a large group of pyridazine derivatives was investigated.[65] It was found that introducing a substituent in the position 3 of the pyridazine cycle

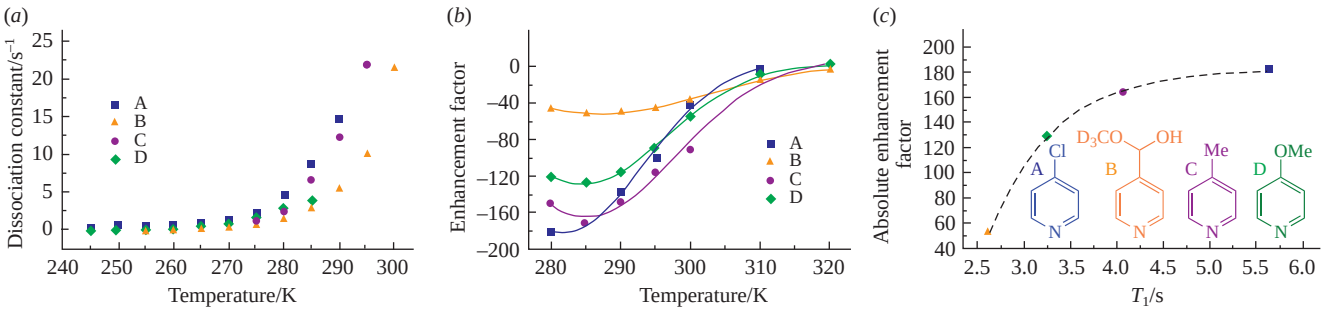

Figure 4 (*a*) Substrate dissociation rate constants as a function of temperature. (*b*) ^{1}H NMR SABRE signal enhancement for the substrate *ortho* protons as a function of temperature. (*c*) Correlation of the absolute signal enhancement at the optimum temperature for each substrate with the corresponding T_1 values. The substrate structures are shown in panel (*c*). Adapted from ref. 63 published under a permissive Creative Commons Attribution 3.0 Unported License CC BY by the Royal Society of Chemistry.

is not detrimental to the SABRE performance due to the alternative possibility of coordination to Ir *via* the N-1 site. On the other hand, 3,6-disubstituted pyridazines were polarized inefficiently or were not polarized at all due to steric constraints. The highest obtained ^{1}H polarization reached 28.7% for 4,5-bis(trideuteromethoxycarbonyl)pyridazine. The structural feature of 3- and 3,6-substituted pyridazine derivatives, namely the presence of near-equivalent protons, was used to create long-lived spin states with lifetimes reaching 113 s at 9.4 T and 255 s at 10 mT (the corresponding T_1 values were 29 and 43 s, respectively).[66]

Importantly, SABRE showed its efficiency for the hyperpolarization of various biologically active compounds. For example, Zeng *et al.* investigated hyperpolarization of tuberculosis drugs isoniazid and pyrazinamide, the derivatives of pyridine and pyrazine heterocycles, respectively.[67] Olaru *et al.* studied ^{1}H SABRE hyperpolarization of nicotinic acid (vitamin B3).[68] The attainable signal enhancements as well as the substrate ^{1}H chemical shifts showed pronounced dependence on pH.

The SABRE ^{1}H polarization levels can be significantly increased by partial replacement of ^{1}H nuclei with deuterium in both the substrate[69–71] and the NHC ligand.[69,72] This effect is associated with both spin dilution (the simple decrease in the number of polarizable spins in the substrate) and an increase in the effective T_1 of the substrate. Tailored partial deuteration of nicotinamide and methyl nicotinate provided a 2–3-fold increase in the attainable ^{1}H polarization compared to their unlabeled isotopologues.[69] Next, the use of the partially deuterated d_{22}-IMes ligand allowed one to obtain up to 26.8% ^{1}H polarization of methyl 4,6-d_2-nicotinate, and the $P_{^1H}$ levels were boosted further to 50% with the use of higher pressure and non-polarizable methyl 2,4,5,6-d_4-nicotinate as a co-ligand.[69] In the later work, screening of a library of partially deuterated NHC ligands enabled further polarization increase to 63%.[72] Similar studies were conducted with selective deuteration of pyridine, methyl isonicotinate, isonicotinamide, methyl pyrazine-2-carboxylate, isoniazid, and pyrazinamide, with the maximal ^{1}H polarizations of 6.7, 7.4, 11.0, 11.9, 4.1, and 2.1%, respectively.[70,71]

SABRE-Relay

The requirement of reversible exchange with a hydride transition metal complex significantly limits the range of molecules amenable to SABRE hyperpolarization. In 2018, Duckett and co-workers developed the SABRE-Relay approach which allows one to hyperpolarize many compounds otherwise inaccessible for SABRE.[73] In SABRE-Relay, the protons of ammonia or an amine RNH_2 are hyperpolarized *via* reversible exchange with a SABRE polarization transfer catalyst (Figure 5). Next, proton exchange of this HP transfer agent with a target molecule polarizes the target. Thus, SABRE-Relay expands the range of SABRE-hyperpolarized compounds to those with exchangeable protons, *e.g.*, alcohols, amides, carboxylic acids, carboxylates, phosphates and others.[73] Moreover, SABRE-Relay is compatible with both ^{1}H and heteronuclear polarization.[73] Importantly, SABRE-Relay requires the use of aprotic solvent, *e.g.* CD_2Cl_2 or $CDCl_3$, instead of the typical for SABRE experiments methanol-d_4.

A theoretical description of SABRE-Relay considering both chemical kinetics and spin dynamics was attempted by Knecht *et al.*[74] The suggested theoretical model made it possible to simulate the dependences of attainable polarization on the system parameters, *e.g.*, the substrate and the amine concentrations, the proton exchange rates and the polarization transfer field. Several experimental studies have been also

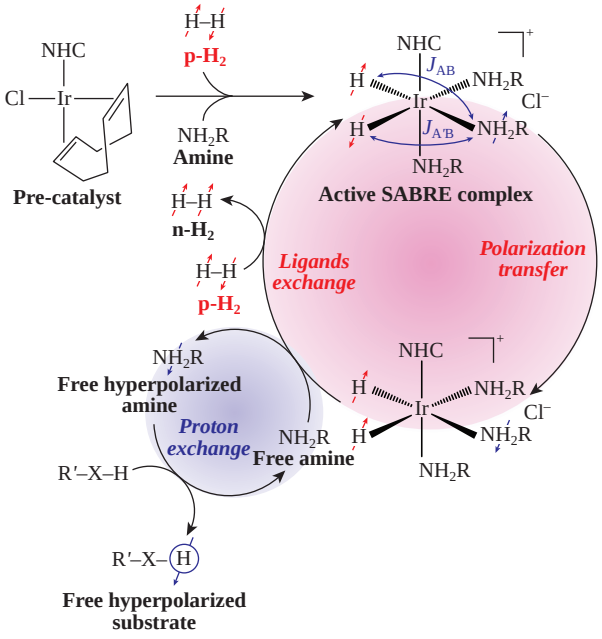

Figure 5 Scheme of polarization transfer and chemical exchange processes in SABRE-Relay.

conducted in recent years, broadening the scope of this approach. Systematic studies revealed that various primary aliphatic amines can be polarized by SABRE and thus can be used as transfer agents in the SABRE-Relay process; however, sterically hindered, aromatic or secondary amines are not polarized at all.[75] Next, a vast library of primary amines was screened as transfer agents for SABRE-Relay polarization employing 1-propanol as a model substrate.[76] The highest ^{1}H NMR signal enhancements were obtained with ammonia and benzylamine-d_7, corresponding to the averaged $P_{^1H}$ = 2.2 and 1.8%, respectively. SABRE-Relay was used for ^{13}C hyperpolarization of ^{13}C- and ^{2}H-isotopically labeled glucose and fructose with $P_{^{13}C}$ of up to 1.1%.[77] It was shown that at millimolar concentrations of D-[$^2H_7$,$^{13}C_6$]glucose its SABRE-Relay-enhanced ^{13}C NMR signal is linearly proportional to its concentration allowing for its quantitative measurement. Moreover, the feasibility of quantification of anomeric α and β forms of glucose and fructose *via* SABRE-Relay was demonstrated. SABRE-Relay was employed for ^{29}Si NMR signal enhancement of silanols; here, hyperpolarization enabled monitoring of the subsequent reaction of silanol with Tf_2O.[78] Finally, a different approach to SABRE-Relay was proposed.[79] Here, an N-heterocyclic substrate (*e.g.*, nicotinamide) is polarized *via* the standard SABRE procedure in the presence of another metal complex (*e.g.*, [Pt(dppp)$(OTf)_2$], dppp = 1,3-bis(diphenylphosphino)propane). The substrate reversibly binds to the second complex, and the use of magnetic field cycling enables polarization transfer to the ^{31}P nuclei of dppp ligand. Further development of this approach may involve reversible coordination of another substrate to the second complex; thus, this second substrate may be hyperpolarized without the direct interaction with the hydride complex exchanging with p-H_2.

Heteronuclear SABRE

Despite the overall higher sensitivity of ^{1}H NMR, hyperpolarization of heteronuclei has several important advantages over ^{1}H hyperpolarization. First of all, heteronuclei often possess significantly longer polarization lifetimes, reaching several[80,81] or even tens[82,83] of minutes. For potential *in vivo* biomedical applications, heteronuclear hyperpolarization is advantageous due to the absence of background signal. Various

heteronuclei have been hyperpolarized so far, including ^{13}C,[84] ^{15}N,[81] ^{19}F,[85] ^{31}P,[86] ^{29}Si[87] and ^{119}Sn.[87]

In principle, hyperpolarization of ^{15}N nuclei can be achieved spontaneously in high-field SABRE experiments *via* cross-relaxation effects, although this approach is inefficient, providing $P_{^{15}N}$ of only less than 0.1%.[88,89] Significantly higher polarization levels can be obtained at high magnetic fields with the use of specially designed radiofrequency (RF) pulse sequences. In fact, this approach was first demonstrated even earlier than the classic low-field ^1H SABRE effects, using PH-INEPT[90] based pulse sequences for the transfer of polarization from the hydrides to the ^{15}N nuclei of coordinated [^{15}N]pyridine.[91] In the following years a number of RF pulse sequences were designed to transfer polarization to ^{15}N nuclei directly bound to the Ir center. In LIGHT-SABRE sequence proposed by Theis *et al*. a long low-power continuous-wave (CW_x) pulse with an amplitude of $2\pi(J_{HH} \pm J_{NN})$ is applied at the resonance frequency of the equatorial-bound substrate ^{15}N nuclei, converting initial singlet order of hydrides into transverse magnetization.[92] This is followed by a soft $\pi/2_y$ pulse which aligns this magnetization along the *z* axis. The sequence of these two pulses is repeated multiple times to build up ^{15}N polarization of free substrate. The use of the second $\pi/2_y$ pulse can be omitted if one performs off-resonant CW irradiation.[93] It was shown that the ongoing singlet–triplet ($S–T_0$) mixing in the active complex reduces the attainable ^{15}N polarization because LIGHT-SABRE simply does not exploit the T_0 state.[93] The remedy is the application of a hard $\pi/2_y$ pulse on the ^1H channel simultaneously with the CW pulse – this modified sequence called SLIC-SABRE boosts the attainable ^{15}N signal enhancement by an order of magnitude compared to LIGHT-SABRE.[93] SLIC-SABRE sequence can be further improved by addition of broad-band ^1H decoupling during the CW pulse.[94] Other approaches exploiting the same idea of bringing the spin system into the LAC regime in the rotating frame were also suggested[95,96] as well as improvements of INEPT-based sequences.[97]

An alternative approach for the transfer of SABRE hyperpolarization to heteronuclei is the use of an appropriate magnetic field at which the hydride protons and heteronuclei are strongly coupled with each other. This field lies in the range from hundreds of nanotesla to several microtesla depending on the target nuclei. This approach called SABRE-SHEATH[98] is rather easy to implement if one has a mu-metal shield available attenuating the Earth's magnetic field. To obtain the maximal polarization levels, a precise control of the microtesla magnetic field is needed that can be achieved by addition of a solenoid inside the magnetic shield with a variable direct current passing through.[99] Typically, SABRE-SHEATH experiments are conducted at a constant ultra-low magnetic field (Figure 6).

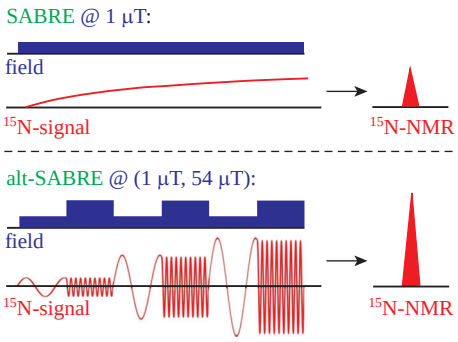

Figure 6 Magnetic field patterns and schematics of corresponding ^{15}N NMR signal evolution in SABRE-SHEATH (top) and alt-SABRE-SHEATH (bottom) experiments. Adapted with permission from ref. 102. Copyright (2021) The Authors. ChemPhysChem published by Wiley-VCH GmbH.

However, recently it was suggested to use alternation between an ultra-low field of ~1 μT or less and a higher field of tens of μT.[100–102] At the ultra-low field, the LAC condition is established and polarization transfers coherently from the hydrides to the heteronuclei. Next, at the higher field spin dynamics in the complex is stopped while chemical exchange continues, allowing the HP substrate molecules to dissociate and the hydride atoms to replenish hyperpolarization *via* replacement with fresh p-H_2. As a result, this alt-SABRE-SHEATH approach increases the attainable polarization levels. Moreover, it was shown that if the substrate dissociation rate is sufficiently fast, the optimal ultra-low field in alt-SABRE-SHEATH sequence is significantly shifted from the LAC conditions.[103] Recently, other improvements were also proposed, such as the use of oscillating magnetic fields along the *z* axis[104] or addition of an oscillating magnetic field along the *x* axis to the ALT-SABRE-SHEATH procedure.[105]

Usually, SABRE-SHEATH provides significantly higher polarization levels for the free substrate molecules than RF-based approaches (although there is a counterexample of 4-amino[^{15}N]pyridine which was polarized to $P_{^{15}N}$ = 4% using SLIC-SABRE[106] and only to $P_{^{15}N}$ = 2% *via* SABRE-SHEATH[107]). Another advantage of SABRE-SHEATH over RF-based methods is its universality: one can use the same procedure to hyperpolarize heteronuclei in the broad range of compounds[81,108] without the need to tailor the experimental parameters to a particular molecule (although recently Lindale *et al*. proposed the broadband X-SABRE RF pulse sequence which overcomes this issue[109]).

Heteronuclear SABRE enables long-lived hyperpolarization of many compounds of potential interest as molecular MRI contrast agents. For example, metronidazole, a nitroimidazole-based antibiotic and hypoxia probe, was hyperpolarized to $P_{^{15}N}$ > 30% (for the ^{15}N-3 site coordinating to the Ir center) using SABRE-SHEATH approach at the natural abundance of ^{15}N nuclei.[110,111] Careful tuning of the Ir catalyst structure provided the increase of ^{15}N polarization level to 54%.[112] The synthesis of isotopically enriched [$^{15}N_3$]metronidazole enabled efficient hyperpolarization of the other two ^{15}N atoms, with ~16% polarization of each of the three ^{15}N sites.[80] Moreover, it was found that in this compound the $^{15}NO_2$ group possesses remarkably long relaxation time reaching 9.7 min at the clinically relevant magnetic field of 1.4 T.[80] A comparative study of $^{15}N_3$- and $^{15}N_2$-isotopologues of metronidazole showed that the presence of quadrupolar ^{14}N nuclei in the latter molecule significantly decreases the attainable SABRE-SHEATH polarization due to efficient scalar relaxation of the second kind at the microtesla magnetic field (Figure 7).[113] Other nitroimidazole-based antibiotics were also successfully polarized using SABRE-SHEATH approach including nimorazole[114] (which is currently under phase 3 clinical study as a radiosensitizer for the treatment of head and neck cancer) and ornidazole.[115] Recently, the similarly impressive results were demonstrated for the nitrile-based anticancer drugs letrozole and anastrozole which were polarized to $P_{^{15}N}$ exceeding 10% at the natural abundance of ^{15}N nuclei using alt-SABRE-SHEATH.[116] Importantly, these compounds possessed remarkably long ^{15}N polarization lifetimes at 1 T field (9.2 and 7.0 min, respectively). Also ^{15}N SABRE-SHEATH was successfully demonstrated for several other anticancer agents,[81] N-heterocyclic antifungal drugs,[117] nicotinamide,[81,118] *etc*.

A highly important recent advance is ^{13}C SABRE-SHEATH hyperpolarization of pyruvate, which is a well-developed molecular HP contrast agent for the MRI studies of prostate cancer.[11,119] It was made feasible by the addition of DMSO as a co-ligand stabilizing the active complex.[120] Later, this approach was extended to other biologically important α-ketocarboxylates,

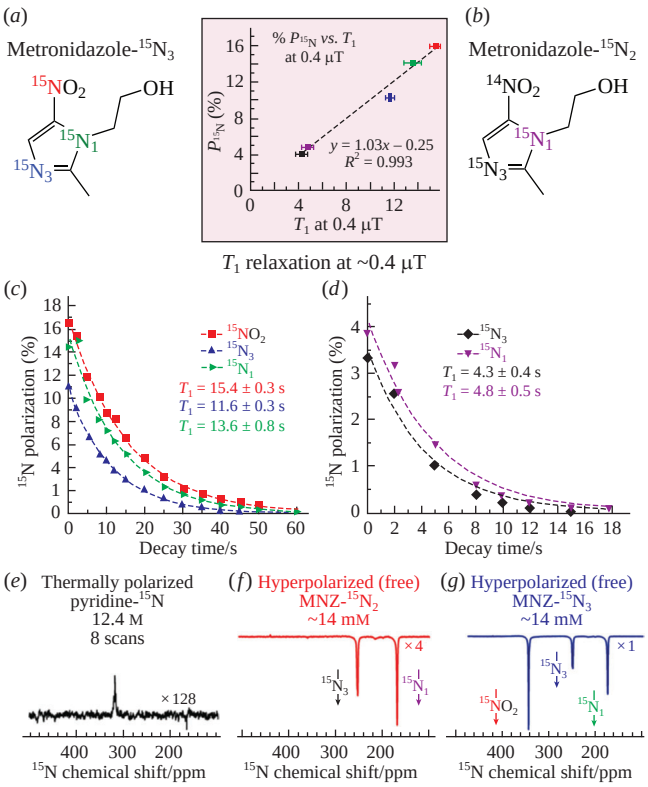

Figure 7 (*a*) and (*b*) Structures of $^{15}N_3$- and $^{15}N_2$-metronidazole isotopologues. (*c*) and (*d*) Corresponding ^{15}N T_1 decay curves at 0.4 μT. (*e*) Reference ^{15}N NMR spectrum of thermally polarized neat [^{15}N]pyridine acquired with 8 signal accumulations. (*f*) and (*g*) Corresponding ^{15}N NMR spectra of HP [$^{15}N_2$]metronidazole and [$^{15}N_3$]metronidazole. The inset shows the linear dependence of $P_{^{15}N}$ on T_1 of the corresponding ^{15}N site. The data were acquired using 2 mM Ir-IMes catalyst and 20 mM total metronidazole concentrations. Adapted with permission from ref. 113. Copyright (2020) The Royal Society of Chemistry.

e.g., ketoisocaproate,[121,122] α-ketoglutarate,[123] and oxalate.[124] The efficiency of ^{13}C SABRE-SHEATH hyperpolarization of pyruvate was boosted using the following temperature cycling procedure.[125,126] First, high ^{13}C polarization of the bound pyruvate was built up at a lower temperature *via* p-H_2 exchange at a microtesla magnetic field. Next, at an elevated temperature the substrate exchange is accelerated providing accumulation of polarization in the ensemble of free pyruvate molecules. As a result, up to 10.8% ^{13}C polarization of free [1-^{13}C]pyruvate was achieved.[125] Later optimization (including the use of the alt-SABRE-SHEATH approach) allowed to increase $P_{^{13}C}$ of [1-^{13}C]-pyruvate to 14.8%.[127] Recently, the application of a weak spin-locking oscillating magnetic field with an 1.8 μT amplitude along the *x* axis at the 50 μT static magnetic field along the *z* axis and deuteration of the [1-^{13}C]pyruvate methyl group provided the record 22% ^{13}C polarization.[128] Also, it has been shown that ^{13}C polarization of pyruvate may be efficiently transferred to protons prior to detection using SLIC RF pulse.[129] This allows one to combine the advantages of both protons and heteronuclei, *i.e.* the longer lifetime of heteronuclear polarization and the wide availability of proton detection in clinical environment.

[1-^{13}C]pyruvate hyperpolarized *via* SABRE-SHEATH in methanol : saline solution was studied *in vivo* as a metabolic marker. The real-time metabolic tracking of the formation of lactate, alanine, pyruvate hydrate, and bicarbonate was shown in rats.[130] However, in this demonstration the toxic methanol and Ir complex remained in the bolus, making this work limitedly applicable for further studies. Another research group independently demonstrated the first biocompatible *in vivo* study using ^{13}C SABRE-hyperpolarized pyruvate.[131] In this work HP [1-^{13}C]pyruvate-d_3 was formulated in aqueous solution and the most of methanol and Ir complex were removed *via* solvent evaporation and metal filtering below acute toxic levels. Further details are presented in the following section of this review.

The longer lifetime of heteronuclear hyperpolarization can be exploited for the use of such HP molecules in the subsequent reactions for kinetic and mechanistic studies. For example, ^{13}C SABRE-SHEATH was employed to monitor [1,2-$^{13}C_2$]-pyruvate decarboxylation to acetic acid and CO_2 under the action of H_2O_2.[132] Bae *et al.* used ^{15}N SABRE-SHEATH to hyperpolarize $^{15}N_4$-1,2,4,5-tetrazine which was then introduced into the bioorthogonal chemistry with a cyclooctyne derivative.[133] The sequence of Diels–Alder and retro-Diels–Alder reactions afforded HP cycloaddition product and HP ortho-$^{15}N_2$ gas. Likely para-$^{15}N_2$ is also formed in this reaction, although it is challenging to prove because para-$^{15}N_2$ is NMR silent similar to p-H_2. Rayner *et al.* exploited co-ligand strategy to yield efficient SABRE-SHEATH hyperpolarization of [^{15}N]nitrite which was then subjected to several transformations.[134] Diazotization of [^{15}N]aniline with HP Na$^{15}NO_2$ yielded [$^{15}N_2$]benzenediazonium which then reacted with sodium [1-^{15}N]azide to form phenyl azide isotopologues *via* phenyl-1*H*-[$^{15}N_3$]pentazole isotopomers. Next, phenyl azide underwent 1,3-dipolar cycloaddition with a cyclooctyne derivative. All these reaction products and intermediates were hyperpolarized despite the relatively fast relaxation of [^{15}N]nitrite with T_1 = 16.5 s at 9.4 T field.[134]

Toward biocompatible SABRE

The essential key in advancing SABRE technique toward preclinical MRI applications is the determination of the toxicology profiles of the SABRE components (activated Ir complex, solvent, and substrate). Several studies addressed those issues *in vitro* and it was found that the dominant factor causing cells death is the Ir complex, even at low concentrations and short exposure times.[135] Moreover, it was shown that changing the ligand environment of the SABRE catalyst does not have a significant influence on the resulting cytotoxicity, which is thus predominantly the result of heavy metal content.[136] In order to achieve biocompatibility, the amount of activated catalyst must be either decreased substantially or completely eliminated. In this regard, the SABRE catalyst separation is imperative for *in vivo* applications.

Recently various approaches have been developed to overcome this issue. It was shown that anchored Ir complexes on solid supports (*via* covalent binding with functionalized polymers, TiO_2/polymer composite or SiO_2) are able to mediate the SABRE process.[137–139] Due to simplicity of the polarization transfer catalyst removal *via* filtration, heterogeneous SABRE can be used to render catalyst-free hyperpolarized solutions. However, this approach is generally inferior to homogeneous SABRE in terms of the attainable polarization levels. For example, for pyridine the highest ^1H signal enhancement factors achieved using heterogeneous SABRE catalysts varied from 5 to 70.[137,138] In the case of heteronuclear SABRE using heterogeneous catalyst, a 100-fold enhancement of ^{15}N NMR signals in [^{15}N]pyridine was observed.[139]

The typical solvents for SABRE are alcohols – methanol and ethanol, however their administration *in vivo* should be minimized due to adverse effects at high concentrations.[135] Recent developments toward a biocompatible SABRE system through approaches aiming to generate an aqueous SABRE-hyperpolarized bolus have been reported. It was found that once activated and dried, the Ir-IMes catalyst is soluble in aqueous media with either pyridine or nicotinamide substrates incorporated into its hexacoordinate structure.[140] SABRE with nicotinamide in D_2O provided ~30-fold ^1H NMR signal enhancements at 9.4 T using this approach, which are twice as

low as those in ethanol-d_6.[140] The modification of NHC ligand with ethylene glycol groups[141–143] is a working approach to increase the solubility of Ir catalyst and perform SABRE in water directly. However, the achieved polarization levels are systematically lower compared to those in alcohols; this can be largely attributed to the reduced solubility of hydrogen in water. Moreover, for *in vivo* applications the Ir complex should be separated from the HP substrate anyway, and the use of water-soluble catalyst makes this even more challenging.

Another promising approach is the so-called catalyst separated hyperpolarization through SABRE or CASH-SABRE.[144] This approach generates an HP bolus in saline media while simultaneously achieving catalyst separation *via* phase transfer. It was demonstrated that the SABRE in biphasic mixture ($CDCl_3/D_2O + NaCl$) provides substantial ^1H NMR signal enhancements for a range of substrates in the aqueous phase, while the Ir catalyst remains mostly in the organic phase with phase separation times of less than 10 s (Figure 8). Other salts (AcONa, $AcONH_4$, NH_4Cl, NaOH, $NaHCO_3$, and Na_2CO_3) also work as phase transfer catalysts but not as efficiently as NaCl.[144] The resulting $P_{^1H}$ of pyrazine, 5-methylpyrimidine, methyl 4,6-d_2-nicotinate, 4,6-d_2-nicotinamide, and pyridazine after complete phase separation were 2.5, 1.1, 9.7, 0.8, and 1.2% (per proton), respectively. Besides, the same method was applied to ^{13}C and ^{15}N SABRE-SHEATH allowing the authors to hyperpolarize pyrazine in aqueous solution with $P_{^{13}C}$ of 0.15% and $P_{^{15}N}$ of 0.98%.[144] The biocompatibility of the resulting HP bolus was also assessed: according to UV spectroscopy results, the residual Ir catalyst concentration in the HP bolus was estimated as less than 1.5 μM. Due to partial solubility of chloroform in water the residual 0.05 vol% chloroform was found.[144] The authors noted that N_2 purge would be needed to lower this concentration in an HP bolus if it was to be used clinically. The approach with the use of a lipophilic resin for the final purification of an HP aqueous bolus can be adapted from the PHIP-SAH method.[145] The cytotoxicity studies were also performed for the aqueous solution derived from biphasic SABRE with deuterated pyrazinamide in the $CD_2Cl_2/D_2O + NaCl$ solution.[136] The cell viability (human cancer cell lines A549 and MCF7) was not altered with the exposure times of up to 24 h. The type of substrate used affects the overall efficiency of CASH-SABRE not only in terms of achievable polarization, but also in terms of the residual Ir concentration, since the solubility of the activated Ir complex in water can vary substantially.[144]

A variation of phase separated SABRE approach (the so-called Re-Dissolution SABRE) was proposed by Schmidt *et al.*[146] Here [1-^{13}C]pyruvate is precipitated from the catalyst-containing methanol media using ethyl acetate addition, and then is rapidly reconstituted in aqueous media. ^{13}C polarization of 9 ± 1% was demonstrated after re-dissolution in water with the residual iridium mass fraction of 8.5 ± 1.5 ppm.

Several studies[147,148] show that after phase separated SABRE there is still a measurable quantity of Ir in the aqueous solution; therefore, an additional purification step is required. An alternative approach for the residual SABRE catalyst removal based on its irreversible binding to solid phase scavengers and subsequent filtration was proposed.[111,147,148] A number of functionalized silicas and polystyrene powders was tested and it was found that nitrogen-containing scavengers show generally poorer performance compared to sulfur-containing ones in terms of overall efficiency and capture rate.[147] Treating 0.5 ml of the aqueous solution of the activated SABRE complex (with pyridine as a ligand) with 100 mg of mercaptopropyl silica for less than 10 s leads to complete capture of the Ir complex from the solution (the measured Ir concentration is less than the ICP-AES detection sensitivity of 0.3 ppb[147]). In another study, direct comparison of several N-containing silicas with a similar silica powder size showed that 3-aminopropyl, 3-(imidazol-1-yl)propyl, and 2-(2-pyridyl) functionalized silica gels are the most efficient.[148] Extrapolation of these results suggests that ~1 g of 2-(2-pyridyl) functionalized silica gel would render iridium below the level detected in blanks for the ICP-AES instrument utilized in this study, with an initial concentration of ~1.7 ppm and an exposure time of ~2 min.

An exciting piece of work was done by de Maissin *et al.*,[131] in which [1-^{13}C]pyruvate-d_3 was successfully hyperpolarized by

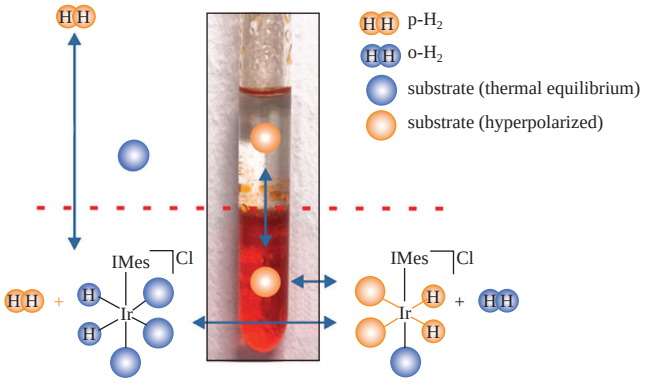

Figure 8 The scheme illustrating the CASH-SABRE approach. The catalyst resides in the organic phase, while the substrate is divided between the two phases according to the principles of phase-transfer catalysis. Adapted with permission from ref. 144. Copyright (2017) The Authors. Published by Wiley-VCH Verlag GmbH & Co. KGaA, Weinheim.

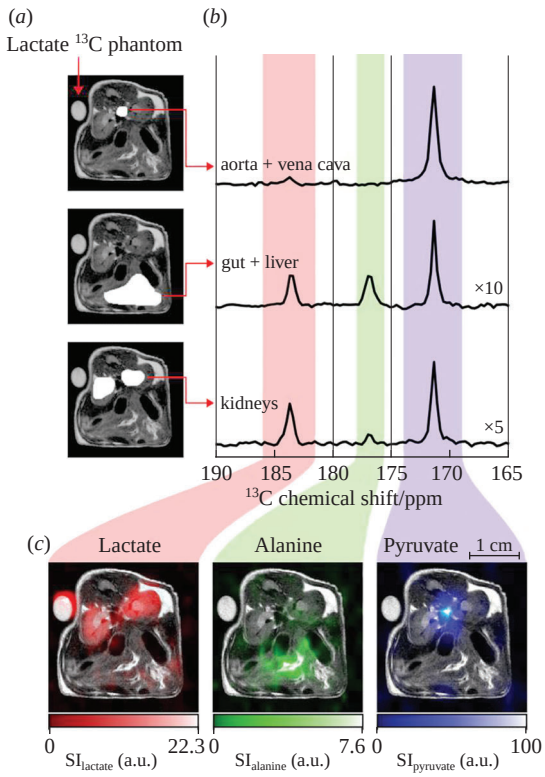

Figure 9 *In vivo* ^{13}C chemical shift imaging of SABRE-hyperpolarized [1-^{13}C]pyruvate-d_3 acquired 15 s after the beginning of the HP bolus injection in a mouse. (*a*) Regions of interests with anatomical ^1H MRI for reference selecting aorta and vena cava (top), the gut and liver (middle), and the kidneys (bottom). (*b*) Corresponding summated ^{13}C NMR spectra from these regions with metabolite ^{13}C signals from pyruvate (blue), alanine (green), and lactate (red). (*c*) 2D metabolite maps of lactate, alanine, and pyruvate (same colors as in (*b*)) superimposed over an anatomical ^1H MR image of the same axial slice. Adapted from ref. 131 published under a permissive Creative Commons license CC BY NC 4.0.

means of SLIC-SABRE at 50 μT field and the long-lived polarization enabled to extract the highly hyperpolarized [1-^{13}C]-pyruvate-d_3 in a purified aqueous solution. The injected solution was sterile, non-toxic, pH neutral and contained ~30 mM [1-^{13}C]-pyruvate-d_3 polarized to ~11% (with residual 250 mM methanol and 20 μM Ir catalyst). It was obtained by the rapid solvent evaporation and the metal complex filtering. Tail-vein administration of the HP bolus and chemical shift imaging (CSI) of pyruvate metabolic conversion in mice enabled metabolic mapping of downstream HP lactate and alanine, demonstrating the translational promise of this approach (Figure 9).

SABRE signal enhancement is usually limited by the p-H_2 concentration in the solution which is relatively low given the low solubility of hydrogen in typical SABRE solvents and the use of moderate hydrogen pressures of several bars. This limitation can be overcome *via* specially designed reactors and automation. Duchowny *et al*. used a high-pressure NMR setup to dramatically increase p-H_2 pressure up to 200 bar.[149] The authors showed that the SABRE signal enhancement grows with pressure eventually reaching the plateau; nevertheless, the use of higher pressure allowed to boost the attainable polarizations by a factor of ~3. Moreover, the feasibility of utilization of liquefied ethane or CO_2 as a solvent for SABRE was demonstrated as a step toward rapid solvent removal and formulation of biocompatible SABRE.[149]

Analytical applications

NMR signal enhancement provided by SABRE has shown its potential for the chemical analysis of complex mixtures. Here we briefly describe these applications and related methodological approaches while more details can be found in the dedicated mini-review by Fraser *et al*.[39] Strong signal enhancement provided by the SABRE technique allows one to dramatically reduce the measurement time required to detect the low-concentrated analytes and establish their chemical structure *via* 1D or 2D NMR spectroscopy.[150] While benefits of SABRE for qualitative analysis are clear, its use for quantitative analysis is more challenging because, in general, the observed signal of an HP substrate is not directly proportional to its concentration. In 2010, Gong *et al*. demonstrated that at the low concentrations of pyridine analyte (*ca*. 0.1–1 mM under the conditions used in that work) the polarization buildup is limited by the substrate and, thus, the SABRE signal is proportional to [Py]. [151] However, this approach has its limitations because at the micromolar substrate concentrations the SABRE signal almost vanishes likely because of the formation of SABRE-inactive complexes (*e.g*., $[Ir(IMes)(Py)_2(CD_3OD)(H)_2]^+$).[152] Eshuis *et al*. showed that this issue can be remedied by the addition of an excess of a suitable co-substrate, *e.g*., 1-methyl-1,2,3-triazole (mtz), which stabilizes the Ir complex in the $[Ir(IMes)(Py)(mtz)_2(H)_2]^+$ form.[152] As a result, quantification of analytes at micromolar concentrations becomes feasible. Using the standard-addition method, this approach was successfully adapted for the quantitative analysis of complex mixtures containing various nitrogen heterocycles and other compounds amenable to SABRE polarization.[153]

A probable overlap of the ^{1}H resonances of analytes in complex mixtures can be surmounted with the use of 2D NMR methods.[154] Eshuis *et al*. proposed the use of the combination of 2D COSY NMR, high-field SABRE and standard-addition method for the quantitative analysis of mixtures.[155] High-field SABRE enables continuous and reproducible polarization of the bound substrate molecules, and 2D COSY makes it possible to observe well-resolved correlations between the signals of aromatic protons of the catalyst-bound analytes and the corresponding hydride resonances. Higher spectral resolution can be achieved with the use of 2D PHIP-ZQ NMR exploiting

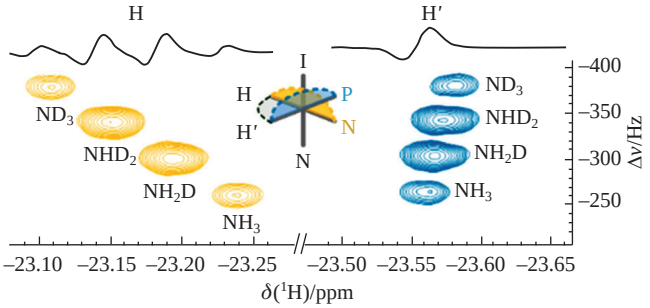

Figure 10 A fragment of a 2D PHIP-ZQ NMR spectrum showing the signals of $[Ir(IMes)(Py)(NH_xD_{3-x})(H)_2]^+$ isotopologue complexes (x = 0, 1, 2, 3) clearly discriminated. Schematic abbreviations of associating ligands are P for pyridine, N for ammonia, and I for IMes. Adapted with permission from ref. 158. Copyright (2022) American Chemical Society.

the remarkably high sensitivity of hydride chemical shifts to the coordinated substrate structure.[156] This approach utilizes non-hydrogenative PHIP rather than SABRE, *i.e*. only the signals of the hyperpolarized hydride protons are analyzed. Importantly, in this case only hydrogen exchange is required while the target substrate can be bound irreversibly.[157] The efficiency of this 2D PHIP-ZQ NMR approach can be illustrated by the discrimination of isotopologues of active SABRE complexes differing only in the degree of substrate deuteration (Figure 10)[158] and the discrimination of D- and L-enantiomers of amino acids.[159] Other recent methodological advances include the combinations of SABRE with 2D DOSY NMR[160] and pure shift NMR,[161] and the use of non-uniform sampling to accelerate the acquisition of 2D PHIP-ZQ NMR spectra.[162]

The developed methodological approaches were successfully employed for the quantitative analysis of biofluids,[156,157,163–165] natural extracts,[166] and food products.[167] The perspectives of the SABRE technique for forensic science were demonstrated by Mewis and co-workers on the example of hyperpolarization of several drug molecules.[168,169] In addition to analytical applications, SABRE has been recently used for reaction monitoring[52,170] and to probe protein–ligand interactions.[171,172]

Instrumentation advances

Typically, SABRE experiments employ manual sample transfer from a polarization transfer field (in the mT or μT range) to an NMR spectrometer for detection. This approach is easy to implement and is widely used in SABRE studies but it is inevitably associated with relatively high experimental errors due to variations in transfer time and magnetic fields experienced by the sample during the transfer. To overcome this issue, various automated SABRE setups were designed which are based on the continuous circulation[173–176] of a SABRE solution (including microfluidic setups[177]) or automated sample shuttling.[178,179]

Usually, SABRE experiments rely on the use of superconducting high-field NMR spectrometers for the signal detection. However, SABRE creates non-equilibrium population of spin energy levels which allows one to detect SABRE signal at fields much lower than several tesla. Low-field NMR offers the advantage of low instrumentation and operational costs compared to traditional high-field NMR based on super-conducting magnets. Also low-field NMR provides higher flexibility in the choice of sample volume and material and allows one to acquire spectra and MR images *in situ* without the sample transfer from the polarization field to the detection field and without the interruption of p-H_2 bubbling through the SABRE solution (because the effects of magnetic susceptibility differences at phase interfaces on the acquired NMR signal are dramatically reduced at low fields).

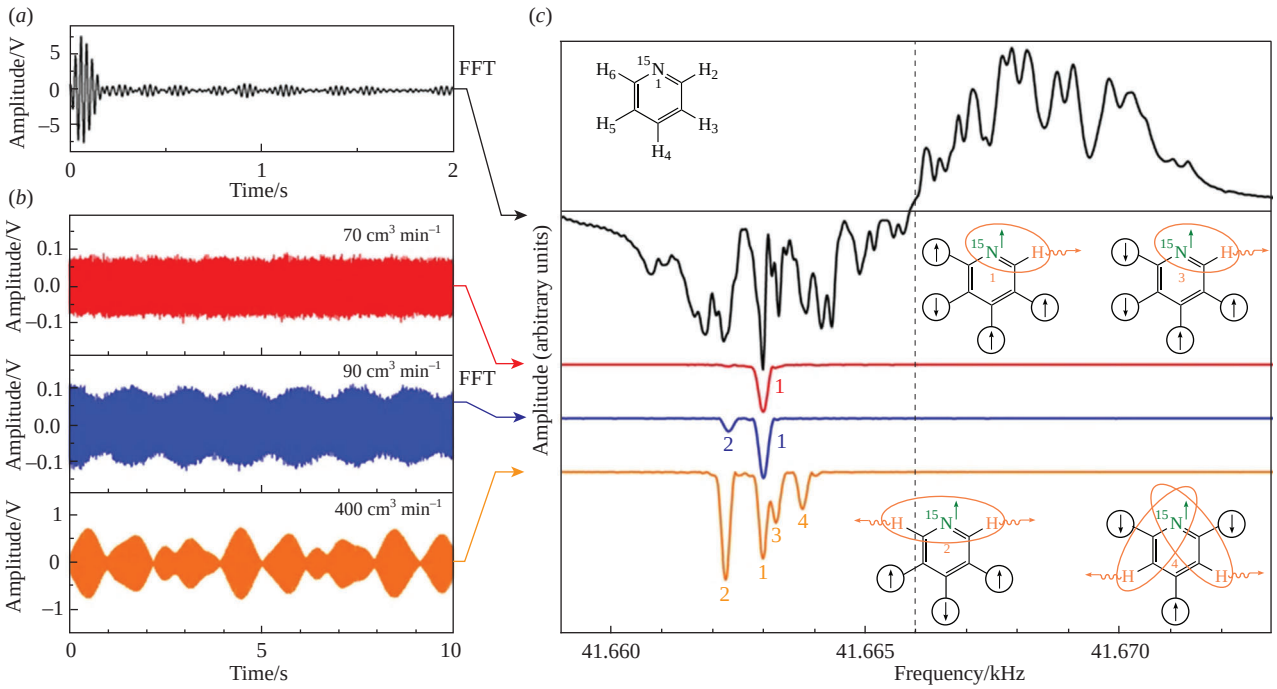

Figure 11 RASER oscillations of [^{15}N]pyridine. (*a*) Initial ^{1}H SABRE signal of [^{15}N]pyridine after 90° pulse excitation. (*b*) ^{1}H RASER signal measured at the p-H_2 flow rates of 70, 90 and 400 cm^3 min^{-1}. (*c*) The corresponding FT NMR spectra show different numbers of RASER modes based on α and β ^{1}H–^{15}N two-spin order, depending on the p-H_2 flow rate. Spin states of [^{15}N]pyridine are shown for the four different modes of oscillation. Adapted with permission from ref. 191. Copyright (2017) Springer Nature.

Recently, benchtop NMR spectrometers based on permanent magnet arrays with magnetic fields of 1–2 T have become readily available. These instruments have shown their utility in a number of SABRE experiments, for example, ^{13}C[126] and ^{15}N[80] SABRE-SHEATH, ^{1}H SABRE with automatic sample shuttling,[178] and continuous flow SABRE and SABRE-SHEATH experiments.[175] Next, SABRE NMR and MRI detection was successfully demonstrated using low-field NMR spectrometers based on electromagnets with fields on the order from several to tens of mT.[180–182] Moreover, it is possible to detect SABRE at zero and ultra-low magnetic fields (ZULF). Superconducting quantum interference device (SQUID) was successfully employed for the SABRE NMR and MRI acquisition at the fields of tens of microtesla.[183–185] Alternatively, SABRE-enhanced NMR at zero and ultra-low magnetic field can be detected using optically-pumped magnetometers.[186–189] The latter approach provides *J*-resolved spectra which are highly characteristic of the HP molecule. Recently, the possibility to detect SABRE-hyperpolarized compounds using nitrogen-vacancy quantum defects in diamond was demonstrated.[190] The optimization of detection protocol allowed one to obtain spectral resolution which is sufficient to measure *J*-couplings.

SABRE-RASER

Recently, it was demonstrated that SABRE hyperpolarization can induce the radio-frequency amplification by stimulated emission of radiation (RASER) effects.[191] The details of the RASER theory can be found elsewhere.[192] In brief, RASER emerges if the radiation damping rate $1/t_{rd}$ is greater than the apparent transverse relaxation rate $1/T_2^*$, where $1/t_{rd}$ is proportional to the quality factor of the resonator (Q) and to the absolute value of the sample magnetization. Moreover, the sample magnetization should originate from the population inversion of spin energy levels. Thus, to initiate the RASER, one should use a high-quality NMR resonator and produce negatively hyperpolarized nuclear spins with high molar polarization. The RASER emission continues as long as sufficiently high population inversion is maintained. The RASER effects manifest themselves as nonlinear interactions between the HP spins and an NMR resonant circuit. For the proof-of-principle RASER observation at 3.915 mT, Suefke *et al*. employed external high-quality factor-enhanced (EHQE)-NMR[193] detector with Q = 300 and [^{15}N]acetonitrile or [^{15}N]pyridine continuously hyperpolarized by SABRE.[191] Fourier transform (FT) of the RASER signal yielded *J*-spectrum with very narrow lines with full width at half maximum (FWHM) of 2.6 mHz. Interestingly, [^{15}N]-pyridine SABRE-RASER gave up to four oscillation modes with different frequencies, and the range of the observed modes depended on the p-H_2 flow rate (Figure 11).[191]

Next, TomHon *et al*. demonstrated the feasibility of the SABRE RASER effects on a commercial 1.1 T benchtop NMR spectrometer and on a 9.4 T superconducting magnet.[175] For this, pyrazine was hyperpolarized by ^{1}H SABRE using a continuous flow automated membrane reactor. Later, pyrazine SABRE RASER was used for the proof-of-principle demonstration of RASER MRI where a small difference in the initial population inversion density inducing RASER was used as a source of MRI contrast.[194]

Conclusions

To summarize, SABRE is a rapidly developing NMR hyperpolarization technique which allows one to boost the sensitivity of NMR and MRI by several orders of magnitude for a broad range of fundamental and practical applications. Methodological advances in SABRE are at the intersection of chemistry and physics with elements of engineering, aimed to applications in biology, medicine and analytical chemistry. The range of substrates amenable to direct SABRE hyperpolarization is continuously growing from nitrogen-containing heterocycles to nitriles, amines, amino acids and carboxylates. Moreover, even broader range of compounds can be added to the list with the SABRE-Relay approach. These advances have become possible due to careful optimization of SABRE chemistry *via* selection of ligand environment of the SABRE-active complex. The studies of SABRE physics allowed one to develop various approaches for conversion of relatively short-lived proton polarization into long-lived heteronuclear polarization at high, low and ultra-low magnetic fields. The recent proof-of-principle *in vivo* studies[130,131] with SABRE-hyperpolarized MRI molecular

contrast agents indicate that SABRE is getting close to practical applications in biology and medicine as a result of all of these methodological advances.

O.G.S. thanks the Council on Grants of the President of the Russian Federation (grant MK-2826.2022.1.3) for the support of reviewing the mechanisms of polarization transfer and chemical exchange in SABRE, SABRE-Relay, analytical applications, instrumental advances and SABRE-RASER. D.B.B. thanks the Russian Science Foundation (grant 21-73-10105) for the support of reviewing heteronuclear SABRE and the methodological advances toward biocompatible SABRE. The authors thank the Russian Ministry of Science and Higher Education for the access to NMR equipment.

References

1 J. Eills, D. Budker, S. Cavagnero, E. Y. Chekmenev, S. J. Elliott, S. Jannin, A. Lesage, J. Matysik, T. Meersmann, T. Prisner, J. A. Reimer, H. Yang and I. V. Koptyug, *Chem. Rev.*, 2023, **123**, 1417.
2 U. L. Günther, in *Modern NMR Methodology*, eds. H. Heise and S. Matthews, Springer, Heidelberg, 2013, pp. 23–70.
3 B. Plainchont, P. Berruyer, J.-N. Dumez, S. Jannin and P. Giraudeau, *Anal. Chem.*, 2018, **90**, 3639.
4 C. R. Bowers and D. P. Weitekamp, *J. Am. Chem. Soc.*, 1987, **109**, 5541.
5 T. C. Eisenschmid, R. U. Kirss, P. P. Deutsch, S. I. Hommeltoft, R. Eisenberg, J. Bargon, R. G. Lawler and A. L. Balch, *J. Am. Chem. Soc.*, 1987, **109**, 8089.
6 R. W. Adams, J. A. Aguilar, K. D. Atkinson, M. J. Cowley, P. I. P. Elliott, S. B. Duckett, G. G. R. Green, I. G. Khazal, J. López-Serrano and D. C. Williamson, *Science*, 2009, **323**, 1708.
7 P. J. Rayner and S. B. Duckett, *Angew. Chem., Int. Ed.*, 2018, **57**, 6742.
8 J. H. Ardenkjaer-Larsen, B. Fridlund, A. Gram, G. Hansson, L. Hansson, M. H. Lerche, R. Servin, M. Thaning and K. Golman, *Proc. Natl. Acad. Sci. USA*, 2003, **100**, 10158.
9 S. J. Elliott, Q. Stern, M. Ceillier, T. El Daraï, S. F. Cousin, O. Cala and S. Jannin, *Prog. Nucl. Magn. Reson. Spectrosc.*, 2021, **126**–**127**, 59.
10 A. C. Pinon, A. Capozzi and J. H. Ardenkjær-Larsen, *Magn. Reson. Mater. Phys., Biol. Med.*, 2021, **34**, 5.
11 J. Kurhanewicz, D. B. Vigneron, J. H. Ardenkjaer-Larsen, J. A. Bankson, K. Brindle, C. H. Cunningham, F. A. Gallagher, K. R. Keshari, A. Kjaer, C. Laustsen, D. A. Mankoff, M. E. Merritt, S. J. Nelson, J. M. Pauly, P. Lee, S. Ronen, D. J. Tyler, S. S. Rajan, D. M. Spielman, L. Wald, X. Zhang, C. R. Malloy and R. Rizi, *Neoplasia*, 2019, **21**, 1.
12 R. L. Hesketh and K. M. Brindle, *Curr. Opin. Chem. Biol.*, 2018, **45**, 187.
13 I. Marco-Rius and A. Comment, *eMagRes*, 2018, **7**, 167.
14 C. R. Bowers and D. P. Weitekamp, *Phys. Rev. Lett.*, 1986, **57**, 2645.
15 B. Chapman, B. Joalland, C. Meersman, J. Ettedgui, R. E. Swenson, M. C. Krishna, P. Nikolaou, K. V. Kovtunov, O. G. Salnikov, I. V. Koptyug, M. E. Gemeinhardt, B. M. Goodson, R. V. Shchepin and E. Y. Chekmenev, *Anal. Chem.*, 2021, **93**, 8476.
16 S. Nantogma, B. Joalland, K. Wilkens and E. Y. Chekmenev, *Anal. Chem.*, 2021, **93**, 3594.
17 Y. Du, R. Zhou, M.-J. Ferrer, M. Chen, J. Graham, B. Malphurs, G. Labbe, W. Huang and C. R. Bowers, *J. Magn. Reson.*, 2020, **321**, 106869.
18 L. Buljubasich, M. B. Franzoni and K. Münnemann, *Top. Curr. Chem.*, 2013, **338**, 33.
19 E. V. Pokochueva, D. B. Burueva, O. G. Salnikov and I. V. Koptyug, *ChemPhysChem*, 2021, **22**, 1421.
20 A. Koch and J. Bargon, *Inorg. Chem.*, 2001, **40**, 533.
21 S. B. Duckett and N. J. Wood, *Coord. Chem. Rev.*, 2008, **252**, 2278.
22 L.-S. Bouchard, S. R. Burt, M. S. Anwar, K. V. Kovtunov, I. V. Koptyug and A. Pines, *Science*, 2008, **319**, 442.
23 E. S. Kononenko, A. I. Svyatova, I. V. Skovpin, L. M. Kovtunova, E. Y. Gerasimov and I. V. Koptyug, *J. Phys. Chem. C*, 2022, **126**, 14914.
24 V. V. Zhivonitko, V.-V. Telkki and I. V. Koptyug, *Angew. Chem., Int. Ed.*, 2012, **51**, 8054.
25 K. Golman, O. Axelsson, H. Jóhannesson, S. Månsson, C. Olofsson and J. S. Petersson, *Magn. Reson. Med.*, 2001, **46**, 1.
26 M. Gierse, L. Nagel, M. Keim, S. Lucas, T. Speidel, T. Lobmeyer, G. Winter, F. Josten, S. Karaali, M. Fellermann, J. Scheuer, C. Müller, F. van Heijster, J. Skinner, J. Löffler, A. Parker, J. Handwerker, A. Marshall, A. Salhov, B. El-Kassem, C. Vassiliou, J. W. Blanchard, R. Picazo-Frutos, J. Eills, H. Barth, F. Jelezko, V. Rasche, F. Schilling, I. Schwartz and S. Knecht, *J. Am. Chem. Soc.*, 2023, **145**, 5960.
27 F. Reineri, T. Boi and S. Aime, *Nat. Commun.*, 2015, **6**, 5858.
28 S. Mamone, A. P. Jagtap, S. Korchak, Y. Ding, S. Sternkopf and S. Glöggler, *Angew. Chem., Int. Ed.*, 2022, **61**, e202206298.
29 K. Them, F. Ellermann, A. N. Pravdivtsev, O. G. Salnikov, I. V. Skovpin, I. V. Koptyug, R. Herges and J. B. Hövener, *J. Am. Chem. Soc.*, 2021, **143**, 13694.
30 S. Alcicek, E. Van Dyke, J. Xu, S. Pustelny and D. A. Barskiy, *Chemistry–Methods*, 2023, **3**, e202200075.
31 A. B. Permin and R. Eisenberg, *J. Am. Chem. Soc.*, 2002, **124**, 12406.
32 R. Zhou, E. W. Zhao, W. Cheng, L. M. Neal, H. Zheng, R. E. Quiñones, H. E. Hagelin-Weaver and C. R. Bowers, *J. Am. Chem. Soc.*, 2015, **137**, 1938.
33 A. Harthun, R. Giernoth, C. J. Elsevier and J. Bargon, *Chem. Commun.*, 1996, 2483.
34 S. R. Muhammad, R. B. Greer, S. B. Ramirez, B. M. Goodson and A. R. Fout, *ACS Catal.*, 2021, **11**, 2011.
35 E. W. Zhao, R. Maligal-Ganesh, Y. Du, T. Y. Zhao, J. Collins, T. Ma, L. Zhou, T.-W. Goh, W. Huang and C. R. Bowers, *Chem*, 2018, **4**, 1387.
36 P. L. Norcott, *J. Am. Chem. Soc.*, 2023, **145**, 9970.
37 D. A. Barskiy, S. Knecht, A. V. Yurkovskaya and K. L. Ivanov, *Prog. Nucl. Magn. Reson. Spectrosc.*, 2019, **114**–**115**, 33.
38 T. B. R. Robertson and R. E. Mewis, in *Annual Reports on NMR Spectroscopy*, ed. G. Webb, Academic Press, 2018, vol. 93, pp. 145–212.
39 R. Fraser, F. P. J. T. Rutjes, M. C. Feiters and M. Tessari, *Acc. Chem. Res.*, 2022, **55**, 1832.
40 G. Buntkowsky, F. Theiss, J. Lins, Y. A. Miloslavina, L. Wienands, A. Kiryutin and A. Yurkovskaya, *RSC Adv.*, 2022, **12**, 12477.
41 B. J. Tickner and V. V. Zhivonitko, *Chem. Sci.*, 2022, **13**, 4670.
42 A. N. Pravdivtsev, G. Buntkowsky, S. B. Duckett, I. V. Koptyug and J.-B. Hövener, *Angew. Chem., Int. Ed.*, 2021, **60**, 23496.
43 R. W. Adams, S. B. Duckett, R. A. Green, D. C. Williamson and G. G. R. Green, *J. Chem. Phys.*, 2009, **131**, 194505.
44 A. N. Pravdivtsev, A. V. Yurkovskaya, H.-M. Vieth, K. L. Ivanov and R. Kaptein, *ChemPhysChem*, 2013, **14**, 3327.
45 A. N. Pravdivtsev, K. L. Ivanov, A. V. Yurkovskaya, P. A. Petrov, H.-H. Limbach, R. Kaptein and H.-M. Vieth, *J. Magn. Reson.*, 2015, **261**, 73.
46 D. A. Barskiy, A. N. Pravdivtsev, K. L. Ivanov, K. V. Kovtunov and I. V. Koptyug, *Phys. Chem. Chem. Phys.*, 2016, **18**, 89.
47 S. Knecht, A. N. Pravdivtsev, J. B. Hövener, A. V. Yurkovskaya and K. L. Ivanov, *RSC Adv.*, 2016, **6**, 24470.
48 A. N. Pravdivtsev and J.-B. Hövener, *Chem. – Eur. J.*, 2019, **25**, 7659.
49 J. R. Lindale, S. L. Eriksson, C. P. N. Tanner and W. S. Warren, *Sci. Adv.*, 2020, **6**, eabb6874.
50 D. A. Barskiy, K. V. Kovtunov, I. V. Koptyug, P. He, K. A. Groome, Q. A. Best, F. Shi, B. M. Goodson, R. V. Shchepin, A. M. Coffey, K. W. Waddell and E. Y. Chekmenev, *J. Am. Chem. Soc.*, 2014, **136**, 3322.
51 S. Knecht, A. S. Kiryutin, A. V. Yurkovskaya and K. L. Ivanov, *J. Magn. Reson.*, 2018, **287**, 74.
52 O. Semenova, P. M. Richardson, A. J. Parrott, A. Nordon, M. E. Halse and S. B. Duckett, *Anal. Chem.*, 2019, **91**, 6695.
53 S. Knecht, S. Hadjiali, D. A. Barskiy, A. Pines, G. Sauer, A. S. Kiryutin, K. L. Ivanov, A. V. Yurkovskaya and G. Buntkowsky, *J. Phys. Chem. C*, 2019, **123**, 16288.
54 M. Fekete, S. S. Roy and S. B. Duckett, *Phys. Chem. Chem. Phys.*, 2020, **22**, 5033.
55 K. Lin, P. TomHon, S. Lehmkuhl, R. Laasner, T. Theis and V. Blum, *ChemPhysChem*, 2021, **22**, 1947.
56 K. D. Atkinson, M. J. Cowley, P. I. P. Elliott, S. B. Duckett, G. G. R. Green, J. López-Serrano and A. C. Whitwood, *J. Am. Chem. Soc.*, 2009, **131**, 13362.
57 M. J. Cowley, R. W. Adams, K. D. Atkinson, M. C. R. Cockett, S. B. Duckett, G. G. R. Green, J. A. B. Lohman, R. Kerssebaum, D. Kilgour and R. E. Mewis, *J. Am. Chem. Soc.*, 2011, **133**, 6134.
58 B. J. A. van Weerdenburg, S. Glöggler, N. Eshuis, A. H. J. (Ton) Engwerda, J. M. M. Smits, R. de Gelder, S. Appelt, S. S. Wymenga, M. Tessari, M. C. Feiters, B. Blümich and F. P. J. T. Rutjes, *Chem. Commun.*, 2013, **49**, 7388.
59 L. S. Lloyd, A. Asghar, M. J. Burns, A. Charlton, S. Coombes, M. J. Cowley, G. J. Dear, S. B. Duckett, G. R. Genov, G. G. R. Green, L. A. R. Highton, A. J. J. Hooper, M. Khan, I. G. Khazal, R. J. Lewis, R. E. Mewis, A. D. Roberts and A. J. Ruddlesden, *Catal. Sci. Technol.*, 2014, **4**, 3544.
60 A. J. Ruddlesden, R. E. Mewis, G. G. R. Green, A. C. Whitwood and S. B. Duckett, *Organometallics*, 2015, **34**, 2997.
61 A. J. Ruddlesden and S. B. Duckett, *Chem. Commun.*, 2016, **52**, 8467.
62 P. Pham and C. Hilty, *Chem. Commun.*, 2020, **56**, 15466.

63 E. V. Stanbury, P. M. Richardson and S. B. Duckett, *Catal. Sci. Technol.*, 2019, **9**, 3914.
64 K. M. Appleby, R. E. Mewis, A. M. Olaru, G. G. R. Green, I. J. S. Fairlamb and S. B. Duckett, *Chem. Sci.*, 2015, **6**, 3981.
65 P. J. Rayner, M. J. Burns, E. J. Fear and S. B. Duckett, *Magn. Reson. Chem.*, 2021, **59**, 1187.
66 S. S. Roy, P. Norcott, P. J. Rayner, G. G. R. Green and S. B. Duckett, *Angew. Chem., Int. Ed.*, 2016, **55**, 15642.
67 H. Zeng, J. Xu, J. Gillen, M. T. McMahon, D. Artemov, J.-M. Tyburn, J. A. B. Lohman, R. E. Mewis, K. D. Atkinson, G. G. R. Green, S. B. Duckett and P. C. M. van Zijl, *J. Magn. Reson.*, 2013, **237**, 73.
68 A. M. Olaru, M. J. Burns, G. G. R. Green and S. B. Duckett, *Chem. Sci.*, 2017, **8**, 2257.
69 P. J. Rayner, M. J. Burns, A. M. Olaru, P. Norcott, M. Fekete, G. G. R. Green, L. A. R. Highton, R. E. Mewis and S. B. Duckett, *Proc. Natl. Acad. Sci. USA*, 2017, **114**, E3188.
70 P. Norcott, M. J. Burns, P. J. Rayner, R. E. Mewis and S. B. Duckett, *Magn. Reson. Chem.*, 2018, **56**, 663.
71 P. Norcott, P. J. Rayner, G. G. R. Green and S. B. Duckett, *Chem. – Eur. J.*, 2017, **23**, 16990.
72 P. J. Rayner, P. Norcott, K. M. Appleby, W. Iali, R. O. John, S. J. Hart, A. C. Whitwood and S. B. Duckett, *Nat. Commun.*, 2018, **9**, 4251.
73 W. Iali, P. J. Rayner and S. B. Duckett, *Sci. Adv.*, 2018, **4**, eaao6250.
74 S. Knecht, D. A. Barskiy, G. Buntkowsky and K. L. Ivanov, *J. Chem. Phys.*, 2020, **153**, 164106.
75 W. Iali, P. J. Rayner, A. Alshehri, A. J. Holmes, A. J. Ruddlesden and S. B. Duckett, *Chem. Sci.*, 2018, **9**, 3677.
76 P. J. Rayner, B. J. Tickner, W. Iali, M. Fekete, A. D. Robinson and S. B. Duckett, *Chem. Sci.*, 2019, **10**, 7709.
77 P. M. Richardson, W. Iali, S. S. Roy, P. J. Rayner, M. E. Halse and S. B. Duckett, *Chem. Sci.*, 2019, **10**, 10607.
78 P. J. Rayner, P. M. Richardson and S. B. Duckett, *Angew. Chem., Int. Ed.*, 2020, **59**, 2710.
79 S. S. Roy, K. M. Appleby, E. J. Fear and S. B. Duckett, *J. Phys. Chem. Lett.*, 2018, **9**, 1112.
80 R. V. Shchepin, J. R. Birchall, N. V. Chukanov, K. V. Kovtunov, I. V. Koptyug, T. Theis, W. S. Warren, J. G. Gelovani, B. M. Goodson, S. Shokouhi, M. S. Rosen, Y.-F. Yen, W. Pham and E. Y. Chekmenev, *Chem. – Eur. J.*, 2019, **25**, 8829.
81 J. F. P. Colell, A. W. J. Logan, Z. Zhou, R. V. Shchepin, D. A. Barskiy, G. X. Ortiz, Jr., Q. Wang, S. J. Malcolmson, E. Y. Chekmenev, W. S. Warren and T. Theis, *J. Phys. Chem. C*, 2017, **121**, 6626.
82 T. Theis, G. X. Ortiz, Jr., A. W. J. Logan, K. E. Claytor, Y. Feng, W. P. Huhn, V. Blum, S. J. Malcolmson, E. Y. Chekmenev, Q. Wang and W. S. Warren, *Sci. Adv.*, 2016, **2**, e1501438.
83 A. S. Kiryutin, V. P. Kozinenko and A. V. Yurkovskaya, *ChemRxiv*, 2023, DOI: 10.26434/chemrxiv-2023-hzk8c.
84 D. A. Barskiy, R. V. Shchepin, C. P. N. Tanner, J. F. P. Colell, B. M. Goodson, T. Theis, W. S. Warren and E. Y. Chekmenev, *ChemPhysChem*, 2017, **18**, 1493.
85 R. V. Shchepin, B. M. Goodson, T. Theis, W. S. Warren and E. Y. Chekmenev, *ChemPhysChem*, 2017, **18**, 1961.
86 V. V. Zhivonitko, I. V. Skovpin and I. V. Koptyug, *Chem. Commun.*, 2015, **51**, 2506.
87 A. M. Olaru, A. Burt, P. J. Rayner, S. J. Hart, A. C. Whitwood, G. G. R. Green and S. B. Duckett, *Chem. Commun.*, 2016, **52**, 14482.
88 A. N. Pravdivtsev, A. V. Yurkovskaya, P. A. Petrov, H.-M. Vieth and K. L. Ivanov, *Appl. Magn. Reson.*, 2016, **47**, 711.
89 K. V. Kovtunov, B. E. Kidd, O. G. Salnikov, L. B. Bales, M. E. Gemeinhardt, J. Gesiorski, R. V. Shchepin, E. Y. Chekmenev, B. M. Goodson and I. V. Koptyug, *J. Phys. Chem. C*, 2017, **121**, 25994.
90 M. Haake, J. Natterer and J. Bargon, *J. Am. Chem. Soc.*, 1996, **118**, 8688.
91 K. D. Atkinson, M. J. Cowley, S. B. Duckett, P. I. P. Elliott, G. G. R. Green, J. Lopez-Serrano, I. G. Khazal and A. C. Whitwood, *Inorg. Chem.*, 2009, **48**, 663.
92 T. Theis, M. Truong, A. M. Coffey, E. Y. Chekmenev and W. S. Warren, *J. Magn. Reson.*, 2014, **248**, 23.
93 S. Knecht, A. S. Kiryutin, A. V. Yurkovskaya and K. L. Ivanov, *Mol. Phys.*, 2019, **117**, 2762.
94 A. N. Pravdivtsev, I. V. Skovpin, A. I. Svyatova, N. V. Chukanov, L. M. Kovtunova, V. I. Bukhtiyarov, E. Y. Chekmenev, K. V. Kovtunov, I. V. Koptyug and J.-B. Hövener, *J. Phys. Chem. A*, 2018, **122**, 9107.
95 A. N. Pravdivtsev, A. V. Yurkovskaya, H. Zimmermann, H.-M. Vieth and K. L. Ivanov, *RSC Adv.*, 2015, **5**, 63615.
96 T. Theis, N. M. Ariyasingha, R. V. Shchepin, J. R. Lindale, W. S. Warren and E. Y. Chekmenev, *J. Phys. Chem. Lett.*, 2018, **9**, 6136.
97 S. Knecht, A. S. Kiryutin, A. V. Yurkovskaya and K. L. Ivanov, *J. Magn. Reson.*, 2018, **287**, 10.
98 T. Theis, M. L. Truong, A. M. Coffey, R. V. Shchepin, K. W. Waddell, F. Shi, B. M. Goodson, W. S. Warren and E. Y. Chekmenev, *J. Am. Chem. Soc.*, 2015, **137**, 1404.
99 R. V. Shchepin, L. Jaigirdar and E. Y. Chekmenev, *J. Phys. Chem. C*, 2018, **122**, 4984.
100 C. P. N. Tanner, J. R. Lindale, S. L. Eriksson, Z. Zhou, J. F. P. Colell, T. Theis and W. S. Warren, *J. Chem. Phys.*, 2019, **151**, 044201.
101 J. R. Lindale, S. L. Eriksson, C. P. N. Tanner, Z. Zhou, J. F. P. Colell, G. Zhang, J. Bae, E. Y. Chekmenev, T. Theis and W. S. Warren, *Nat. Commun.*, 2019, **10**, 395.
102 A. N. Pravdivtsev, N. Kempf, M. Plaumann, J. Bernarding, K. Scheffler, J. B. Hövener and K. Buckenmaier, *ChemPhysChem*, 2021, **22**, 2381.
103 S. L. Eriksson, J. R. Lindale, X. Li and W. S. Warren, *Sci. Adv.*, 2022, **8**, eabl3708.
104 X. Li, J. R. Lindale, S. L. Eriksson and W. S. Warren, *Phys. Chem. Chem. Phys.*, 2022, **24**, 16462.
105 S. L. Eriksson, M. W. Mammen, C. W. Eriksson, J. R. Lindale and W. S. Warren, *J. Magn. Reson.*, 2022, **342**, 107282.
106 A. I. Trepakova, I. V. Skovpin, N. V. Chukanov, O. G. Salnikov, E. Y. Chekmenev, A. N. Pravdivtsev, J.-B. Hövener and I. V. Koptyug, *J. Phys. Chem. Lett.*, 2022, **13**, 10253.
107 N. V. Chukanov, O. G. Salnikov, I. A. Trofimov, M. S. H. Kabir, K. V. Kovtunov, I. V. Koptyug and E. Y. Chekmenev, *ChemPhysChem*, 2021, **22**, 960.
108 A. S. Kiryutin, A. V. Yurkovskaya, P. A. Petrov and K. L. Ivanov, *Magn. Reson. Chem.*, 2021, **59**, 1216.
109 J. R. Lindale, S. L. Eriksson and W. S. Warren, *Phys. Chem. Chem. Phys.*, 2022, **24**, 7214.
110 D. A. Barskiy, R. V. Shchepin, A. M. Coffey, T. Theis, W. S. Warren, B. M. Goodson and E. Y. Chekmenev, *J. Am. Chem. Soc.*, 2016, **138**, 8080.
111 B. E. Kidd, J. L. Gesiorski, M. E. Gemeinhardt, R. V. Shchepin, K. V. Kovtunov, I. V. Koptyug, E. Y. Chekmenev and B. M. Goodson, *J. Phys. Chem. C*, 2018, **122**, 16848.
112 M. Fekete, F. Ahwal and S. B. Duckett, *J. Phys. Chem. B*, 2020, **124**, 4573.
113 J. R. Birchall, M. S. H. Kabir, O. G. Salnikov, N. V. Chukanov, A. Svyatova, K. V. Kovtunov, I. V. Koptyug, J. G. Gelovani, B. M. Goodson, W. Pham and E. Y. Chekmenev, *Chem. Commun.*, 2020, **56**, 9098.
114 O. G. Salnikov, N. V. Chukanov, A. Svyatova, I. A. Trofimov, M. S. H. Kabir, J. G. Gelovani, K. V. Kovtunov, I. V. Koptyug and E. Y. Chekmenev, *Angew. Chem., Int. Ed.*, 2021, **60**, 2406.
115 W. Iali, G. A. I. Moustafa, L. Dagys and S. S. Roy, *Magn. Reson. Chem.*, 2021, **59**, 1199.
116 K. MacCulloch, A. Browning, P. TomHon, S. Lehmkuhl, E. Y. Chekmenev and T. Theis, *Anal. Chem.*, 2023, **95**, 7822.
117 K. MacCulloch, P. Tomhon, A. Browning, E. Akeroyd, S. Lehmkuhl, E. Y. Chekmenev and T. Theis, *Magn. Reson. Chem.*, 2021, **59**, 1225.
118 R. V. Shchepin, D. A. Barskiy, D. M. Mikhaylov and E. Y. Chekmenev, *Bioconjugate Chem.*, 2016, **27**, 878.
119 S. J. Nelson, J. Kurhanewicz, D. B. Vigneron, P. E. Z. Larson, A. L. Harzstark, M. Ferrone, M. van Criekinge, J. W. Chang, R. Bok, I. Park, G. Reed, L. Carvajal, E. J. Small, P. Munster, V. K. Weinberg, J. H. Ardenkjaer-larsen, A. P. Chen, R. E. Hurd, L.-I. Odegardstuen, F. J. Robb, J. Tropp and J. A. Murray, *Sci. Transl. Med.*, 2013, **5**, 198ra108.
120 W. Iali, S. S. Roy, B. J. Tickner, F. Ahwal, A. J. Kennerley and S. B. Duckett, *Angew. Chem., Int. Ed.*, 2019, **58**, 10271.
121 B. J. Tickner, F. Ahwal, A. C. Whitwood and S. B. Duckett, *ChemPhysChem*, 2021, **22**, 13.
122 I. Adelabu, M. R. H. Chowdhury, S. Nantogma, C. Oladun, F. Ahmed, L. Stilgenbauer, M. Sadagurski, T. Theis, B. M. Goodson and E. Y. Chekmenev, *Metabolites*, 2023, **13**, 200.
123 I. Adelabu, J. Ettedgui, S. M. Joshi, S. Nantogma, M. R. H. Chowdhury, S. McBride, T. Theis, V. R. Sabbasani, M. Chandrasekhar, D. Sail, K. Yamamoto, R. E. Swenson, M. C. Krishna, B. M. Goodson and E. Y. Chekmenev, *Anal. Chem.*, 2022, **94**, 13422.
124 S. S. Roy, W. Iali, G. A. I. Moustafa and M. H. Levitt, *Chem. Commun.*, 2022, **58**, 2291.
125 P. TomHon, M. Abdulmojeed, I. Adelabu, S. Nantogma, M. S. H. Kabir, S. Lehmkuhl, E. Y. Chekmenev and T. Theis, *J. Am. Chem. Soc.*, 2022, **144**, 282.

126 I. Adelabu, P. TomHon, M. S. H. Kabir, S. Nantogma, M. Abdulmojeed, I. Mandzhieva, J. Ettedgui, R. E. Swenson, M. C. Krishna, T. Theis, B. M. Goodson and E. Y. Chekmenev, *ChemPhysChem*, 2022, **23**, 131.
127 S. Nantogma, S. L. Eriksson, I. Adelabu, I. Mandzhieva, A. Browning, P. TomHon, W. S. Warren, T. Theis, B. M. Goodson and E. Y. Chekmenev, *J. Phys. Chem. A*, 2022, **126**, 9114.
128 A. B. Schmidt, J. Eills, L. Dagys, M. Gierse, M. Keim, S. Lucas, M. Bock, I. Schwartz, M. Zaitsev, E. Y. Chekmenev and S. Knecht, *J. Phys. Chem. Lett.*, 2023, **14**, 5305.
129 I. Mandzhieva, I. Adelabu, E. Y. Chekmenev and T. Theis, *ACS Sensors*, 2022, **7**, 3773.
130 K. MacCulloch, A. Browning, D. G. Bedoya, S. J. McBride, M. B. Abdulmojeed, C. Dedesma, B. M. Goodson, M. S. Rosen, E. Y. Chekmenev, Y.-F. Yen, P. TomHon and T. Theis, *J. Magn. Reson. Open*, 2023, 100129.
131 H. de Maissin, P. R. Groß, O. Mohiuddin, M. Weigt, L. Nagel, M. Herzog, Z. Wang, R. Willing, W. Reichardt, M. Pichotka, L. Heß, T. Reinheckel, H. J. Jessen, R. Zeiser, M. Bock, D. von Elverfeldt, M. Zaitsev, S. Korchak, S. Glöggler, J.-B. Hövener, E. Y. Chekmenev, F. Schilling, S. Knecht and A. B. Schmidt, *Angew. Chem., Int. Ed.*, 2023, e202306654.
132 B. J. Tickner, P. J. Rayner and S. B. Duckett, *Anal. Chem.*, 2020, **92**, 9095.
133 J. Bae, Z. Zhou, T. Theis, W. S. Warren and Q. Wang, *Sci. Adv.*, 2018, **4**, eaar2978.
134 P. J. Rayner, M. Fekete, C. A. Gater, F. Ahwal, N. Turner, A. J. Kennerley and S. B. Duckett, *J. Am. Chem. Soc.*, 2022, **144**, 8756.
135 A. Manoharan, P. J. Rayner, W. Iali, M. J. Burns, V. H. Perry and S. B. Duckett, *ChemMedChem*, 2018, **13**, 352.
136 A. Manoharan, P. J. Rayner, M. Fekete, W. Iali, P. Norcott, V. H. Perry and S. B. Duckett, *ChemPhysChem*, 2019, **20**, 285.
137 F. Shi, A. M. Coffey, K. W. Waddell, E. Y. Chekmenev and B. M. Goodson, *Angew. Chem., Int. Ed.*, 2014, **53**, 7495.
138 F. Shi, A. M. Coffey, K. W. Waddell, E. Y. Chekmenev and B. M. Goodson, *J. Phys. Chem. C*, 2015, **119**, 7525.
139 K. V. Kovtunov, L. M. Kovtunova, M. E. Gemeinhardt, A. V. Bukhtiyarov, J. Gesiorski, V. I. Bukhtiyarov, E. Y. Chekmenev, I. V. Koptyug and B. M. Goodson, *Angew. Chem., Int. Ed.*, 2017, **56**, 10433.
140 M. L. Truong, F. Shi, P. He, B. Yuan, K. N. Plunkett, A. M. Coffey, R. V. Shchepin, D. A. Barskiy, K. V. Kovtunov, I. V. Koptyug, K. W. Waddell, B. M. Goodson and E. Y. Chekmenev, *J. Phys. Chem. B*, 2014, **118**, 13882.
141 P. Spannring, I. Reile, M. Emondts, P. P. M. Schleker, N. K. J. Hermkens, N. G. J. van der Zwaluw, B. J. A. van Weerdenburg, P. Tinnemans, M. Tessari, B. Blümich, F. P. J. T. Rutjes and M. C. Feiters, *Chem. – Eur. J.*, 2016, **22**, 9277.
142 J. F. P. Colell, M. Emondts, A. W. J. Logan, K. Shen, J. Bae, R. V. Shchepin, G. X. Ortiz, P. Spannring, Q. Wang, S. J. Malcolmson, E. Y. Chekmenev, M. C. Feiters, F. P. J. T. Rutjes, B. Blümich, T. Theis and W. S. Warren, *J. Am. Chem. Soc.*, 2017, **139**, 7761.
143 S. Lehmkuhl, M. Emondts, L. Schubert, P. Spannring, J. Klankermayer, B. Blümich and P. P. M. Schleker, *ChemPhysChem*, 2017, **18**, 2426.
144 W. Iali, A. M. Olaru, G. G. R. Green and S. B. Duckett, *Chem. – Eur. J.*, 2017, **23**, 10491.
145 O. Bondar, E. Cavallari, C. Carrera, S. Aime and F. Reineri, *Catal. Today*, 2022, **397**–**399**, 94.
146 A. B. Schmidt, H. de Maissin, I. Adelabu, S. Nantogma, J. Ettedgui, P. TomHon, B. M. Goodson, T. Theis and E. Y. Chekmenev, *ACS Sensors*, 2022, **7**, 3430.
147 D. A. Barskiy, L. A. Ke, X. Li, V. Stevenson, N. Widarman, H. Zhang, A. Truxal and A. Pines, *J. Phys. Chem. Lett.*, 2018, **9**, 2721.
148 T. B. R. Robertson, L. J. Clarke and R. E. Mewis, *Molecules*, 2022, **27**, 332.
149 A. Duchowny, J. Denninger, L. Lohmann, T. Theis, S. Lehmkuhl and A. Adams, *Int. J. Mol. Sci.*, 2023, **24**, 2465.
150 L. S. Lloyd, R. W. Adams, M. Bernstein, S. Coombes, S. B. Duckett, G. G. R. Green, R. J. Lewis, R. E. Mewis and C. J. Sleigh, *J. Am. Chem. Soc.*, 2012, **134**, 12904.
151 Q. Gong, A. Gordji-Nejad, B. Blümich and S. Appelt, *Anal. Chem.*, 2010, **82**, 7078.
152 N. Eshuis, N. Hermkens, B. J. A. van Weerdenburg, M. C. Feiters, F. P. J. T. Rutjes, S. S. Wijmenga and M. Tessari, *J. Am. Chem. Soc.*, 2014, **136**, 2695.
153 N. Eshuis, B. J. A. van Weerdenburg, M. C. Feiters, F. P. J. T. Rutjes, S. S. Wijmenga and M. Tessari, *Angew. Chem., Int. Ed.*, 2015, **54**, 1481.
154 V. Daniele, F. X. Legrand, P. Berthault, J. N. Dumez and G. Huber, *ChemPhysChem*, 2015, **16**, 3413.
155 N. Eshuis, R. L. E. G. Aspers, B. J. A. van Weerdenburg, M. C. Feiters, F. P. J. T. Rutjes, S. S. Wijmenga and M. Tessari, *Angew. Chem., Int. Ed.*, 2015, **54**, 14527.
156 L. Sellies, I. Reile, R. L. E. G. Aspers, M. C. Feiters, F. P. J. T. Rutjes and M. Tessari, *Chem. Commun.*, 2019, **55**, 7235.
157 L. Sellies, R. L. E. G. Aspers, M. C. Feiters, F. P. J. T. Rutjes and M. Tessari, *Angew. Chem., Int. Ed.*, 2021, **60**, 26954.
158 E. Vaneeckhaute, J.-M. Tyburn, J. G. Kempf, J. A. Martens and E. Breynaert, *J. Phys. Chem. Lett.*, 2022, **13**, 3516.
159 L. Dreisewerd, R. L. E. G. Aspers, M. C. Feiters, F. P. J. T. Rutjes and M. Tessari, *J. Am. Chem. Soc.*, 2023, **145**, 1518.
160 I. Reile, R. L. E. G. Aspers, J.-M. Tyburn, J. G. Kempf, M. C. Feiters, F. P. J. T. Rutjes and M. Tessari, *Angew. Chem., Int. Ed.*, 2017, **56**, 9174.
161 D. A. Taylor, L. S. Natrajan, M. Nilsson and R. W. Adams, *Magn. Reson. Chem.*, 2021, **59**, 1244.
162 R. L. E. G. Aspers and M. Tessari, *Magn. Reson. Chem.*, 2021, **59**, 1236.
163 I. Reile, N. Eshuis, N. K. J. Hermkens, B. J. A. van Weerdenburg, M. C. Feiters, F. P. J. T. Rutjes and M. Tessari, *Analyst*, 2016, **141**, 4001.
164 N. Reimets, K. Ausmees, S. Vija and I. Reile, *Anal. Chem.*, 2021, **93**, 9480.
165 K. Ausmees, N. Reimets and I. Reile, *Chem. Commun.*, 2022, **58**, 463.
166 N. K. J. Hermkens, N. Eshuis, B. J. A. van Weerdenburg, M. C. Feiters, F. P. J. T. Rutjes, S. S. Wijmenga and M. Tessari, *Anal. Chem.*, 2016, **88**, 3406.
167 N. K. J. Hermkens, R. L. E. G. Aspers, M. C. Feiters, F. P. J. T. Rutjes and M. Tessari, *Magn. Reson. Chem.*, 2018, **56**, 633.
168 T. B. R. Robertson, N. Gilbert, O. B. Sutcliffe and R. E. Mewis, *ChemPhysChem*, 2021, **22**, 1059.
169 T. Tennant, M. C. Hulme, T. B. R. Robertson, O. B. Sutcliffe and R. E. Mewis, *Magn. Reson. Chem.*, 2020, **58**, 1151.
170 H. J. Jeong, S. Min, J. Baek, J. Kim, J. Chung and K. Jeong, *ACS Meas. Sci. Au*, 2023, **3**, 134.
171 R. Mandal, P. Pham and C. Hilty, *Chem. Sci.*, 2021, **12**, 12950.
172 R. Mandal, P. Pham and C. Hilty, *Anal. Chem.*, 2022, **94**, 11375.
173 R. E. Mewis, K. D. Atkinson, M. J. Cowley, S. B. Duckett, G. G. R. Green, R. A. Green, L. A. R. Highton, D. Kilgour, L. S. Lloyd, J. A. B. Lohman and D. C. Williamson, *Magn. Reson. Chem.*, 2014, **52**, 358.
174 S. Lehmkuhl, M. Wiese, L. Schubert, M. Held, M. Küppers, M. Wessling and B. Blümich, *J. Magn. Reson.*, 2018, **291**, 8.
175 P. M. TomHon, S. Han, S. Lehmkuhl, S. Appelt, E. Y. Chekmenev, M. Abolhasani and T. Theis, *ChemPhysChem*, 2021, **22**, 2526.
176 P. Štěpánek, C. Sanchez-Perez, V.-V. Telkki, V. V. Zhivonitko and A. M. Kantola, *J. Magn. Reson.*, 2019, **300**, 8.
177 L. Bordonali, N. Nordin, E. Fuhrer, N. Mackinnon and J. G. Korvink, *Lab Chip*, 2019, **19**, 503.
178 F. Ellermann, P. Saul, J.-B. Hövener and A. N. Pravdivtsev, *Anal. Chem.*, 2023, **95**, 6244.
179 A. S. Kiryutin, A. V. Yurkovskaya, H. Zimmermann, H.-M. Vieth and K. L. Ivanov, *Magn. Reson. Chem.*, 2018, **56**, 651.
180 S. Lehmkuhl, M. Suefke, A. Kentner, Y.-F. Yen, B. Blümich, M. S. Rosen, S. Appelt and T. Theis, *J. Chem. Phys.*, 2020, **152**, 184202.
181 D. A. Barskiy, K. V. Kovtunov, I. V. Koptyug, P. He, K. A. Groome, Q. A. Best, F. Shi, B. M. Goodson, R. V. Shchepin, M. L. Truong, A. M. Coffey, K. W. Waddell and E. Y. Chekmenev, *ChemPhysChem*, 2014, **15**, 4100.
182 S. Glöggler, R. Müller, J. Colell, M. Emondts, M. Dabrowski, B. Blümich and S. Appelt, *Phys. Chem. Chem. Phys.*, 2011, **13**, 13759.
183 K. Buckenmaier, M. Rudolph, C. Back, T. Misztal, U. Bommerich, P. Fehling, D. Koelle, R. Kleiner, H. A. Mayer, K. Scheffler, J. Bernarding and M. Plaumann, *Sci. Rep.*, 2017, **7**, 13431.
184 S.-J. Lee, K. Jeong, J. H. Shim, H. J. Lee, S. Min, H. Chae, S. K. Namgoong and K. Kim, *Sci. Rep.*, 2019, **9**, 12422.
185 K. Buckenmaier, K. Scheffler, M. Plaumann, P. Fehling, J. Bernarding, M. Rudolph, C. Back, D. Koelle, R. Kleiner, J. B. Hövener and A. N. Pravdivtsev, *ChemPhysChem*, 2019, **20**, 2823.
186 T. Theis, M. P. Ledbetter, G. Kervern, J. W. Blanchard, P. J. Ganssle, M. C. Butler, H. D. Shin, D. Budker and A. Pines, *J. Am. Chem. Soc.*, 2012, **134**, 3987.
187 J. W. Blanchard, B. Ripka, B. A. Suslick, D. Gelevski, T. Wu, K. Münnemann, D. A. Barskiy and D. Budker, *Magn. Reson. Chem.*, 2021, **59**, 1208.
188 P. Put, S. Alcicek, O. Bondar, Ł. Bodek, S. Duckett and S. Pustelny, *Commun. Chem.*, 2023, **6**, 131.

189 E. T. Van Dyke, J. Eills, R. Picazo-Frutos, K. F. Sheberstov, Y. Hu, D. Budker and D. A. Barskiy, *Sci. Adv.*, 2022, **8**, eabp9242.
190 N. Arunkumar, D. B. Bucher, M. J. Turner, P. TomHon, D. Glenn, S. Lehmkuhl, M. D. Lukin, H. Park, M. S. Rosen, T. Theis and R. L. Walsworth, *PRX Quantum*, 2021, **2**, 010305.
191 M. Suefke, S. Lehmkuhl, A. Liebisch, B. Blümich and S. Appelt, *Nat. Phys.*, 2017, **13**, 568.
192 S. Appelt, A. Kentner, S. Lehmkuhl and B. Blümich, *Prog. Nucl. Magn. Reson. Spectrosc.*, 2019, **114**–**115**, 1.
193 M. Suefke, A. Liebisch, B. Blümich and S. Appelt, *Nat. Phys.*, 2015, **11**, 767.
194 S. Lehmkuhl, S. Fleischer, L. Lohmann, M. S. Rosen, E. Y. Chekmenev, A. Adams, T. Theis and S. Appelt, *Sci. Adv.*, 2022, **8**, eabp8483.

Received: 15th June 2023; Com. 23/7193